THESIS FOR THE DEGREE OF DOCTOR OF PHILOSOPHY

Solids Flow in Large-Scale Circulating Fluidized Bed Furnaces

TOVE DJERF

Solids Flow in Large-Scale Circulating Fluidized Bed Furnaces
TOVE DJERF
ISBN 978-91-7905-511-0

Department of Space, Earth and Environment
Division of Energy Technology
Chalmers University of Technology
SE-412 96 Gothenburg
Sweden
Telephone + 46 (0)31-772 1000

Cover:
[Fluid-dynamical scaling with Glicksman simplified scaling laws,
between small cold laboratory unit and large hot CFB boiler,
se section 2.3 for further details.
- CFB boiler figure with permission from Valmet Technologies Oy]

To all my loved ones, here and above

"Murphy's law or the fourth law of thermodynamics states:
If anything can go wrong, it will!"

– *Anne Roe, The making of a Scientist, 1953*

Solids Flow in Large-Scale Circulating Fluidized Bed Furnaces
TOVE DJERF
Division of Energy Technology
Department of Space, Earth and Environment
Chalmers University of Technology

ABSTRACT

The flow pattern of solids established in large-scale circulating fluidized bed (CFB) furnaces is of great importance for the performance of commercial CFB boilers, as it governs the heat transfer and mixing of the fuel and any other reactive solids. The solids flow pattern in the riser is crucial for the design and scaling up of large-scale CFB technologies for the thermochemical conversion of solids. The aim of this work is to acquire new knowledge and understanding of the solids flow patterns in CFBs that are representative of large-scale furnaces. The goal is to improve the reliability of predictive modeling tools and, thereby expand the development of new and existing CFB technologies within the energy field. The solids flow of a CFB furnace is characterized by a bottom region with a high concentration of solids, a splash zone with strong solids back-mixing, and a transport zone that covers the major height of the furnace and has a lower level of solids back-mixing, from the bottom and upwards.

This thesis uses experimental campaigns and various modeling tools to elucidate the CFB solids flow. The experimental work is carried out in two cold units: a pseudo-2-dimensional unit that allows visual observation of the flow; and a 3-dimensional unit that can be operated under fluid-dynamical scaling, which has been shown to reflect accurately the solids flow in an existing reference >200-MW$_{th}$ CFB boiler. Furthermore, the data derived from the different sizes and operational ranges of these experimental units are linked to previous measurements of large-scale CFB combustion. Examinations of the solids back-mixing phenomena are supported by different modeling tools, including Direct Number Simulations, semi-empirical modeling through the Finite Volume Method, and Monte Carlo modeling.

The results of this work show that: (i) the presence/absence of a dense bottom bed affects the extent of solids entrainment from the bottom region; (ii) a fluid-dynamical region similar to the splash zone is established even in the absence of a dense bottom bed; (iii) the rate of solids back-mixing in the splash zone can be predicted from modeling of the gravity-driven ballistic trajectories; (iv) the solids back-mixing in the transport zone is governed by the transfer of solids through the core-wall layer boundary, which is driven by turbophoresis (i.e., the migration of particles in the direction of increasing particle concentration), and for which a Sherwood number-based expression is proposed that improves on the former empirical expressions; and (v) the solids back-flow effect at the riser exit cannot generally be neglected when predicting the in-furnace back-flow, and is substantial at gas velocities that are typical for commercial CFB boilers. Validated expressions are proposed for the decay coefficients of the splash and transport zones and the solids entrainment from the bottom region. Taking together this collected knowledge, this thesis improves the reliability of semi-empirical modeling tools for the prediction of the solids flow patterns in large-scale CFB furnaces for a wide range of operational conditions.

Keywords: *Circulating fluidized bed boilers, Solids flow, Fluid-dynamical down-scaling, Dense bed, Splash zone, Transport zone*

ACKNOWLEDGMENTS

Last but not least, my biggest supporters are the members of my family, who have had to endure a lot to help me accomplish this, but we fight till the end. Dad – you left an enormous hole that nobody can ever fill but I will always be grateful for the unconditional love you gave and I still feel your support. Mum – You are always there and cheering me on, asking questions about my work and supporting me at every step, reminding me not to forget to relax and enjoy life. My not-so-little brother, Pontus – always helping and trying to make everyone happy, I love you, so don't forget to do what you want sometimes. Lotti and Håkan – thanks for giving me some peace of mind and space to just relax.

Love of my life, Sebastian, there are no words for what you give me. I can only be thankful that it is you who is sitting beside me in the roller-coaster that is our life. I'm looking forward to the rest of our life together. Theodor, our joy and hurricane, Mommy loves you!

Yours truly!   ***Tove***

LIST OF PUBLICATIONS

This thesis is based on the following papers, which are referred to in the thesis according to their Roman numerals:

I.   T. Karlsson, X. Liu, D. Pallarès, F. Johnsson
     Solids circulation in circulating fluidized beds with low riser aspect ratio and varying total solids inventory
     Powder Technology 316 (2017): 670–676

II. T. Djerf, D. Pallarès, F. Johnsson
     Bottom-bed fluid dynamics – Influence on solids entrainment
     Fuel Processing Technology 173 (2018): 112–118

III. T. Djerf, D. Pallarès, F. Johnsson
     Solids flow pattern in large-scale CFB boilers: experimental evaluation at fluid-dynamical downscaled conditions
     Chemical Engineering Science 231 (2021): 116309

IV. T. Djerf, D. Pallarès, F. Johnsson
     Fluid dynamics of the splash zone in large-scale circulating fluidized bed boilers
     Submitted for publication

V.   T. Djerf, D. Pallarès, F. Johnsson, G. Sardina, H. Ström
     Solids back-mixing in the transport zone of circulating fluidized bed boilers
     Submitted for publication

Tove Djerf (formerly, Karlsson) is the main researcher for all the papers. Associate Professor David Pallarès and Professor Filip Johnsson have contributed with guidance in the experimental work, discussions, writing and editing of the papers. Dr. Xuemin Lui (Tsinghua University) has contributed with experimental work to Paper I. Associate Professor Gaetano Sardina has performed the CFD modeling in Paper V and co-authored the methods section. Associate Professors Gaetano Sardina and Henrik Ström have also contributed to Paper V through discussions and editing of the paper.

TABLE OF CONTENTS

CHAPTER 1
Introduction

Mitigation of climate change and the ongoing search for reliable energy supplies drive to a large extent current technical development in the heat and power sector. The need for such developments is made clear in the IEA's Summary Insight of 2016, which lists higher efficiency, a larger share of renewables, and significant use of carbon capture and storage (CCS) as important elements in the pathways to achieve the goals set out in the Paris Agreement [1]. The combination of renewable fuel conversion and CCS (abbreviated as BECCS, Bio Energy CCS, for the case of biogenic fuels) represents a strategy for ensuring net-negative emissions of CO_2 to the atmosphere. The future of fossil fuel combustion is feasible only if combined with the CCS technology, so as to comply with the emissions targets set out in the Paris Agreement. Several carbon capture technologies have been developed, among which oxyfuel combustion, chemical looping combustion, and post-combustion capture are foreseen to play significant roles in the future energy system. However, the implementation of these measures will require increased capital investments and operational costs and will decrease plant efficiency. Regarding renewable fuels, although an increase in the general use of biomass is envisioned as a pathway to decreased net CO_2 emissions, the heat and power sector will need to compete with other sectors for the available biomass feedstock [2]. It seems likely that this competition will restrict the future pool of renewable fuels for the heat and power sector to low-grade biomass and biogenic waste fractions, in particular since an increased awareness of the sustainability of biofuels can be expected. Low-grade biomass fuels can be problematic in terms of agglomeration, slag formation, corrosion, and the formation of nitrogen oxide species (NO_x) during combustion, and they require strong knowledge of the process for efficient usage. In addition, the reactors that will be used for converting biogenic fuels are expected to be smaller in size than coal-fired CFB furnaces because the former reactors: (i) are typically applied in combined heat and power plants in district heating systems; and (ii) suffer from limitations linked to transport logistics, given the low energy densities of biogenic feedstocks. In addition, biomass-fired units are typically limited in steam data due to the risk of high-temperature corrosion of heat transfer surfaces as a result of alkali compounds released from the fuel, which is one of the main challenges in the conversion of low-grade fuels [3, 4].

Furthermore, increases in non-dispatchable renewable energy in the forms of wind and solar power are expected to generate a greater need for load flexibility of dispatchable electricity, i.e., the need for efficient flexible operation at different load levels in conjunction with smooth transitions between these load levels.

In light of the above, the fluidized bed (FB) technology – commonly used for the thermochemical conversion (combustion, gasification and pyrolysis) of solid fuels – is foreseen as an important technology in the future energy system, owing to its high fuel flexibility, relatively high mixing rates, and the possibility for in-bed emissions control through the use of active bed materials [3-5]. Initially, FB boilers were designed to operate at gas velocities below the terminal velocity of the bed material (i.e., without significant entrainment of the bed material), in so-called bubbling fluidized beds (BFB). Owing to their investment costs, such BFB units have been in sustained commercial operation for unit sizes >10 MW_{th} [4]. Such boilers are typically applied in combined heat and power plants up to a size (currently around 100 MW_e [3]) that is set by design limitations and the competing CFB alternative. For improved economy, extended range of operation and better performance at larger scales, an increase in the specific thermal capacity (MW/m^2) was achieved through the use of higher gas velocities. As this entailed significant entrainment of the bed material from the bottom region of the boiler, a solids recirculation system had to be implemented, thereby creating so-called circulating fluidized bed (CFB) units. CFB boilers have a higher investment cost than BFBs and are economically feasible for commercialization at scales >30 MW_{th} [4] (although the Chalmers 12-MW_{th} CFB boiler is run on a commercial basis), with most commercial CFB boilers ranging from >100 MW_{th} (when used in combined heat and power schemes) to around 1,400 MW_{th} (i.e., up to 520 MW_e [3]) when used as power boilers. To ensure sufficient heat transfer, a CFB boiler of high capacity requires an external heat exchanger in the loop seal (or an additional heat transfer element – wing walls - in the furnace). CFB units are characterized by favorable gas-solids contacts and relatively high thermal mixing and inertia, providing relatively homogeneous fields of temperature and heat extraction.

Given the above characteristics, the CFB technology is envisioned to contribute to the future energy system through different applications, some of which are listed below as examples:

- The implementation of dual FB systems for:
  - chemical looping combustion for carbon capture [6]
  - indirect gasification to produce high-quality biogas [7, 8]
  - calcium looping for carbon capture [9]
- The use of active bed materials for:
  - improved conversion of low-grade fuels, e.g., oxygen carrier-aided combustion [10]
  - thermochemical energy storage processes [11, 12]
- The application of compact oxyfuel furnace designs for carbon capture [13, 14]

Even if CFB should be the preferred technology for these applications, there is a lack of detailed knowledge regarding the solids flow and mixing patterns in large-scale CFB reactors.

Acquisition of this knowledge is crucial for enabling reliable scale-up and design of the reactor systems, since the solids flow and mixing patterns govern the mass and heat transport within the CFB reactors. Since most of the experimental work on CFB reactors to date has been carried out under ambient conditions at small scales, and in order to provide access to *in situ* measurements and to limit experimental costs, there is a need to perform measurements under conditions relevant for large-scale CFB reactors, so as to understand the influence of unit size and how the solids flow and mixing patterns can be scaled [15]

Reaching a better understanding the phenomena governing the solids flow in a CFB reactor could theoretically be achieved by analyzing the outputs from modeling the CFB solids flow from first principles, i.e., computational fluid-dynamics (CFD). However, such modeling is currently limited, since it either requires excessive computational effort (for the Lagrangian description of each solid particle) or contains highly uncertain formulations for some terms in the governing equations (for the Eulerian description of the solids phase as a continuum) [16]. Instead, semi-empirical modeling has been commonly used in the development of the CFB technology. In this type of modeling, knowledge of the CFB is based on experimental data (see [17-25]), which are used to formulate hypotheses and models for the macroscopic flow fields [26-29], instead of solving the momentum equations for the solids and gas phases. The validity of such semi-empirical models is, therefore, restricted to the range of parameters for which the measurements supporting the semi-empirical expressions were developed. Thus, there is an urgent need for more-generic semi-empirical expressions that broaden the validity range of such models. Furthermore, in order to provide a basis for predictive modeling, semi-empirical expressions must aim to require only those input parameters that are known and adjustable during design/operation.

1.1   Aim and Scope

The aim of this thesis is to extend current understanding of the solids flow pattern in the riser of CFB units representing conditions that can be applied to commercial-scale units for the thermochemical conversion of solid fuels. More specifically, the objectives of this work are to identify, characterize and evaluate the mechanisms underlying the different solids back-mixing phenomena that govern the solids flow patterns in CFB furnaces, i.e., dense bed depletion, solids entrainment from the bottom region, back-mixing in the splash and transport zones, and the back-flow in the riser exit. An additional objective is to combine this acquired knowledge so as to develop and validate expressions that can be used to describe key in-furnace phenomena and, thereby, close the solids mass balance in the riser, i.e., predict the solids flows throughout the CFB furnace. Combined with the solids velocity, this would also allow prediction of the solids concentration profile.

The expected impact of this work is the establishment of more-reliable semi-empirical models for the design, scale-up and optimization of large-scale CFB boilers or reactors within the defined scope (see below). Furthermore, this work is expected to support the validation and development of CFD modeling by providing new knowledge and high-quality measurements that are relevant for large-scale CFB combustion.

As indicated above, the scope of the work is restricted to geometries and conditions relevant to large-scale CFB boilers. The characteristics of such units are: bed solids of Geldart Group B type; geometries with a furnace aspect ratio in the order of ≤10; operation yielding a dense bed with an aspect ratio <1 (resulting in non-slugging conditions); and an external circulation rate of solids that is <20 kg/m^{2}s. In this thesis, the use of the terms *particles, solids, particulate phase*, refers to the bulk bed material conforming the vast majority of the solids inventory in CFB boilers. Thus, the fuel particles are assumed not to influence the solids flow, as they are a small fraction of the total inventory.

1.2   Methodology

Semi-empirical modeling is used in this work to advance the understanding of the solids mixing flow. This modeling strategy presents an obvious challenge in terms of formulating general hypotheses that are valid for a wide range of CFB furnace sizes and operational conditions, as opposed to describing a specific operational interval in a particular unit. Thus, as indicated in the previous section, validation of modeling that involves broad ranges of unit sizes and operational conditions is of critical importance and, therefore, depends directly on the availability of the relevant experimental data. Very few datasets derived from commercial CFB boilers have been published for the following reasons: *in situ* measurements are difficult and costly to perform, the available grid of data sampling locations yields an unsatisfactory resolution, and commercial CFB boiler technologies are subject to trade secrecy policies.

This work addresses the existing knowledge gap related to CFB boiler solids flows by expanding the size and operational ranges of the analysis through dedicated experimental analyses of the solids flows in two different units operated under ambient conditions. Initially, a pseudo-2-dimensional CFB unit is used. Thereafter, a fluid-dynamically down-scaled cold-flow model (validated to reproduce the hot solids flow in the reference >200-MW$_{th}$ CFB boiler) is employed to generate comprehensive and accurate experimental data across a broad operational range, both under scaled and non-scaled conditions. The measurements in this work use pressure sampling (for the solids concentration along the riser height) and fluidization of the cyclone leg to measure the external solids circulation. The measurements are complemented with published data from large-scale CFB boilers. Different types of modeling are used to study specific phenomena: Monte Carlo modeling of solids trajectories is applied to evaluate statistically the solids back-mixing rate in the splash zone, while Direct Numerical Simulation (DNS) is used to gain insights into the solids flow in the boundary between the core region and the wall layer in the transport zone. Semi-empirical modeling is used to translate the gained experimental knowledge into mathematical expressions and thereafter combine these expression for the overall prediction of the solids flow in the CFB riser.

1.3   Outline of the papers

An overview of the contents of the papers in this thesis is presented in Figure 1. Each paper can be briefly summarized as follows:

- **Paper I** describes an initial assessment of the solids flow phenomena in the riser of a CFB furnace, with special focus on the bottom region and the depletion of the dense bed. The analysis of the results is limited to a qualitative framework, since a pseudo-2-dimensional unit is employed.

- **Paper II** presents the first results obtained from the dedicated 3-dimensional unit that was designed and built for the work of this thesis. The unit is dimensioned according to scaling laws. However, this work uses a non-scaled bed material, which allowed acquaintance to be made with the unit and facilitated a first study of the solids fluid-dynamics applying less-challenging handling and operational procedures.

- **Paper III** studies the solids flow in the riser established in the fluid-dynamically down-scaled cold-flow model when it is operated with flows and bed material according to scaling laws, such that it resembles the reference large-scale boiler. This provides values that are representative of commercial CFB boilers and, therefore, results that have quantitative relevance.

- **Paper IV** focuses on the solids flow in the splash zone, using collated measurement data from **Papers I-III** and earlier published data from the Chalmers 12-MW$_{th}$ CFB boiler. The paper explores both the solids back-mixing rate (proposing a simple model for its prediction) and the solids flux that is effectively entrained into the transport zone (for which a semi-empirical expression is derived).

- **Paper V** focuses on the solids flow in the transport zone, based on data from **Paper III** and data from the literature on large-scale CFB boilers. The underlying mechanisms governing the solids back-mixing are evaluated by combining these experimental data with closures of the 3-dimensional mass balance for the solids in the core region and DNS modeling of the core-to-layer solids transfer. As a result, the core-to-layer mass transfer coefficient is found to govern the back-mixing, and a Sherwood number-based expression is derived that provides general good agreement with the set of measurement data used.
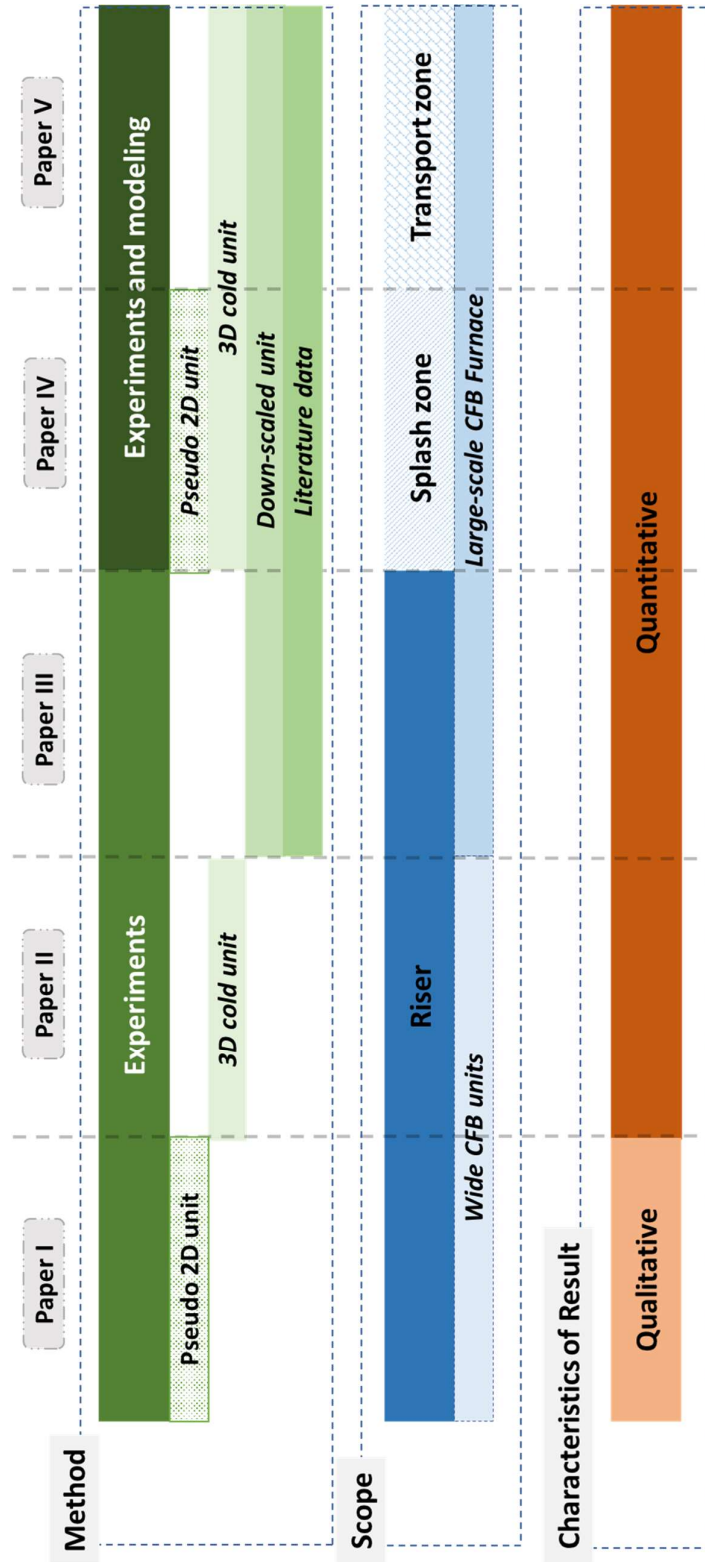
Figure 1. Overview of the papers in this thesis and their knowledge accumulation scheme

CHAPTER 2
Theory

2.1   Solids flow pattern in large-scale CFB furnaces

The solids flow pattern in FBs has been studied extensively over many years. FBs representative of large-scale CFB boilers typically contain a dense bottom bed with gas bubbles, which when they erupt at the dense bed surface eject material upwards into the freeboard [30, 31]. These ejected particles from the dense bottom bed consist of two phases which co-exist along the furnace height: a cluster phase mostly falling back down onto the dense bed surface – generating the so-called *splash zone* - and a dispersed phase, which is effectively entrained from the bottom region the upper *transport zone* [31]. Although by definition the cluster phase dominates the splash zone and the dispersed phase dominates the transport zone [17], it is reasonable to assume that there is some exchange of solids between the two phases (it is most likely that some of the solids in the clusters are transferred to the dispersed phase). The entrained solids flow upwards in the form of a core flow (F_{entr} in Figure 2) as they partially back-mix along the furnace (F_{lat} in Figure 2) through transfer to the down-flowing solids layers formed by the furnace walls [20] (F_{layer} in Figure 2). Once they reach the riser exit, the solids can be internally circulated into the wall layers through the back-flow effect ($F_{backflow}$ in Figure 2) or be externally recirculated through the cyclone and seal system (F_s in Figure 2), eventually returning to the bottom of the riser [17, 23, 31-33]. This solids flow scheme is depicted in Figure 2 together with the three different fluid-dynamical zones typically established in a CFB boiler [17], i.e. the bottom region consisting of the dense bottom bed located directly above the primary gas distributor and the splash zone immediately above it. The latter, together with the transport zone occupied by the disperse phase form the so-called *freeboard*.

$$F_{entr} = C_{s,entr}(u_g - u_t)A$$

$$F_{top} = C_{s,entr}e^{-K(H-H_b)}(u_g - u_t)A$$

$$F_{lat} = C_{s,entr}(1 - e^{-K(H-H_b)})(u_g - u_t)A$$

$$F_s = C_{s,entr}e^{-K(H-H_b)}(u_g - u_t)(1 - k_b)A$$

$$F_{backflow} = C_{s,entr}e^{-K(H-H_b)}(u_g - u_t)k_bA$$

$$F_{layer} = C_{s,entr}(u_g - u_t)A \\ -C_{s,entr}e^{-K(H-H_b)}(u_g - u_t)(1 - k_b)A$$
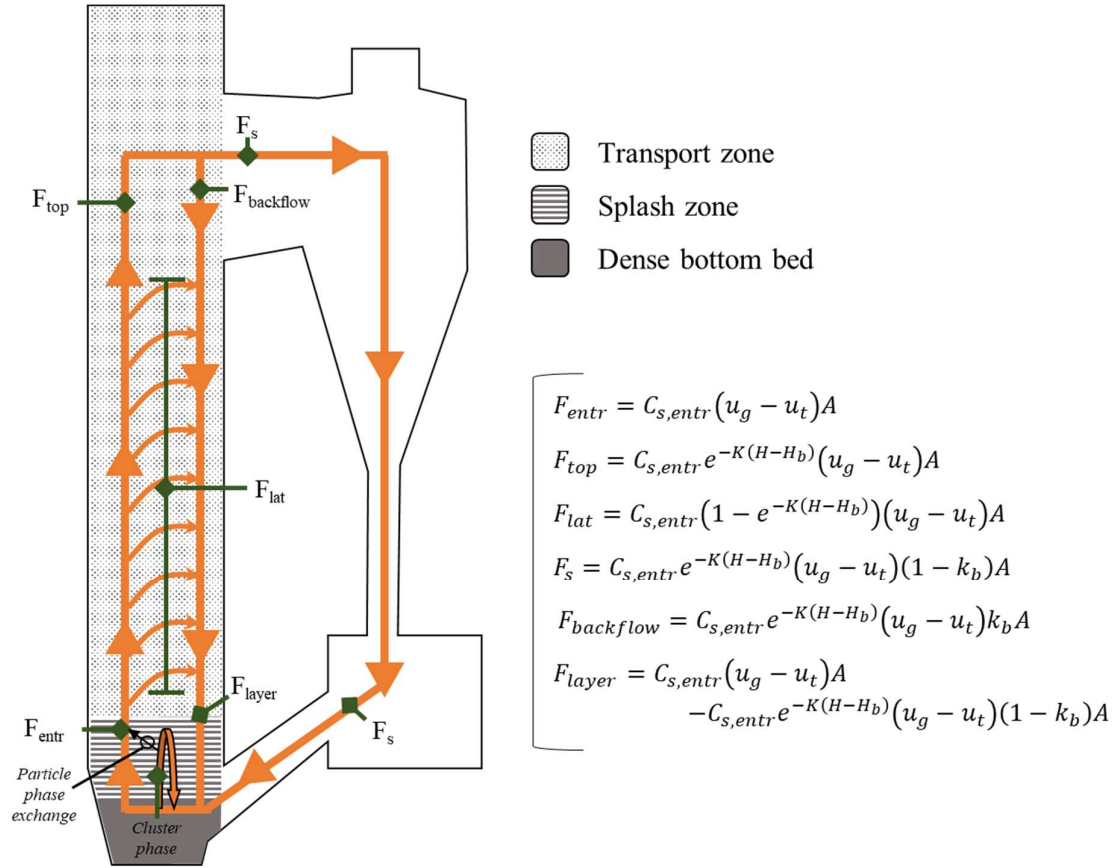
Figure 2. Schematics of the solids flow in a CFB boiler.

The solids flow pattern established in large-scale CFB furnaces described above and depicted in Figure 2 yields a vertical profile of solids concentration revealing the three fluid-dynamical regions (dense bottom bed, splash zone and transport zone) as illustrated in Figure 3. Based on the solids flow pattern described above, the expressions describing the solids concentration in each of these three regions are presented below.

A dense region similar to a bubbling bed is typically established at the bottom of CFB furnaces [34], even though in a CFB boiler the fluidization velocity exceeds the terminal velocity of most of the solids inventory. This is attributed to the strong local fluctuations in gas velocity that is inherent to FBs and enhanced by the limited pressure drop across the gas distributor [35] typically applied in commercial units to decrease the operational fan costs. Based on this, the dense bed of CFB boilers has been shown to contain bubbles of the exploding type [36, 37]. The time-averaged cross-sectional solids flux in the dense bed is zero, since the same flow of solids that is ejected from the dense bed is recycled back to the dense bed through the different solids back-mixing phenomena in the furnace and the external recirculation of solids. This results in a constant time-averaged solids concentration over its height, yielding a linear pressure drop with height. Thus:

$$C_s(h \le H_b) = C_{s,H_b} \tag{1}$$

.

In relative terms, the solids concentration in the dense bed of large-scale CFB boilers is typically within the interval ε_s=0.52–0.66 [36], and semi-empirical expressions for its prediction are available [38]. The height of the dense bed is dependent upon the amount and properties of the bed material in the CFB loop and the fluidization velocity applied [36]. Under some conditions, e.g., for a sufficiently high primary gas velocity and/or sufficiently low furnace pressure drop, the dense bed may be depleted.

A splash zone develops above the dense bed as bubble eruptions at the dense bed surface eject clustered solids into the freeboard. These clusters are not dragged up by the gas into the upper furnace locations but falls back into the dense bed, i.e. representing the main back-mixing process in the splash zone as indicated by the back-circulating arrow in Figure 2. These flows of ejected and back-mixed cluster solids are believed to be large (yielding a high thermal mixing in the splash zone). Only a small share of the ejected cluster solids will be transferred to the disperse phase and entrained the transport zone. This is concluded from visual observation in cold models and measurements in large-scale CFB boilers [17] which yield splash zones with a solids concentration profile similar to those in units at bubbling conditions which has no net solids entrainment up through and out of the furnace, i.e. no or little solids entrainment from the splash zone. The splash zone follows a steep exponential decay in solids concentration [17, 39]

$$C_{cluster}(h > H_b) = C_{cluster}]_{H_b} \ e^{-a(h-H_b)} \tag{2}$$

Where the decay coefficient, *a*, is often described [8, 38, 40-43] as:

$$a \propto \frac{u_g}{u_t} \tag{3}$$

In the transport zone, the solids back-mixing can be described as a net lateral flow from the upwards core flux into the downward-flowing wall layers (F_{lat} in Figure 2). The back-mixing change in flow can be described as:

$$dF_{disperse} = - K \ F_{disperse} \ dh \tag{4}$$

where the solids are assumed to be disperse and thus flow according to their single particle terminal velocity. This terminal velocity can be assumed to be constant with height in the riser (note that this assumption neglects the size segregation effect of the solids back-mixing in this region, which affects the mean terminal velocity). Thus, the upwards dispersed phase flow may be described as:

$$F_{disperse} = C_{disperse}(u_g - u_t)A \tag{5}$$

Based on this, integration of Eq. (4) results in an exponential decay in solids concentration of the disperse solids phase, characterized by a decay coefficient, *K* [17] and the initial condition given by the concentration of entrained solids at the dense bed surface, $C_{s,entr}$ (see Figure 3):

$$C_{disperse}(h > H_b) = C_{s,entr} \ e^{-K(h-H_b)} \tag{6}$$

The concentration of solids entrained from the bottom bed is obtained from the extrapolation of the upper solids concentration profile to the dense bed height, H_b (or in the absence of a dense bed, down to the bottom grid) (see Figure 3) [44, 45]. The decay coefficient often takes the following form [17, 38, 40-43, 46, 47]:

$$K \propto \frac{1}{u_g - u_t} \tag{7}$$

In line with the above assumption that the two solids phases co-exist, the time-averaged cross-sectional solids concentration is assumed to be the sum of Eqs. (2) and (6), such that:

$$C_s(h) = \left(C_{s,H_b} - C_{s,entr}\right)e^{-a(h-H_b)} + C_{s,entr}e^{-K(h-H_b)} \tag{8}$$

where the concentration of clusters at the dense bed surface, $C_{cluster}]_{H_b}$, equals by continuity the difference between the solids concentration in the dense bed and the concentration of entrained solids, $C_{s,H_b} - C_{s,entr}$.

Accounting for the three fluid-dynamical regions discussed above, the vertical profile of solids concentration along the riser can be described with Eqs. (8) and (1) and is exemplified in Figure 3:

$$C_s(h) = \begin{cases} \left(C_{s,H_b} - C_{s,entr}\right)e^{-a(h-H_b)} + C_{s,entr}e^{-K(h-H_b)} & \forall\ h > H_b \\ C_{s,H_b} & \forall\ h \le H_b \end{cases} \tag{9}$$
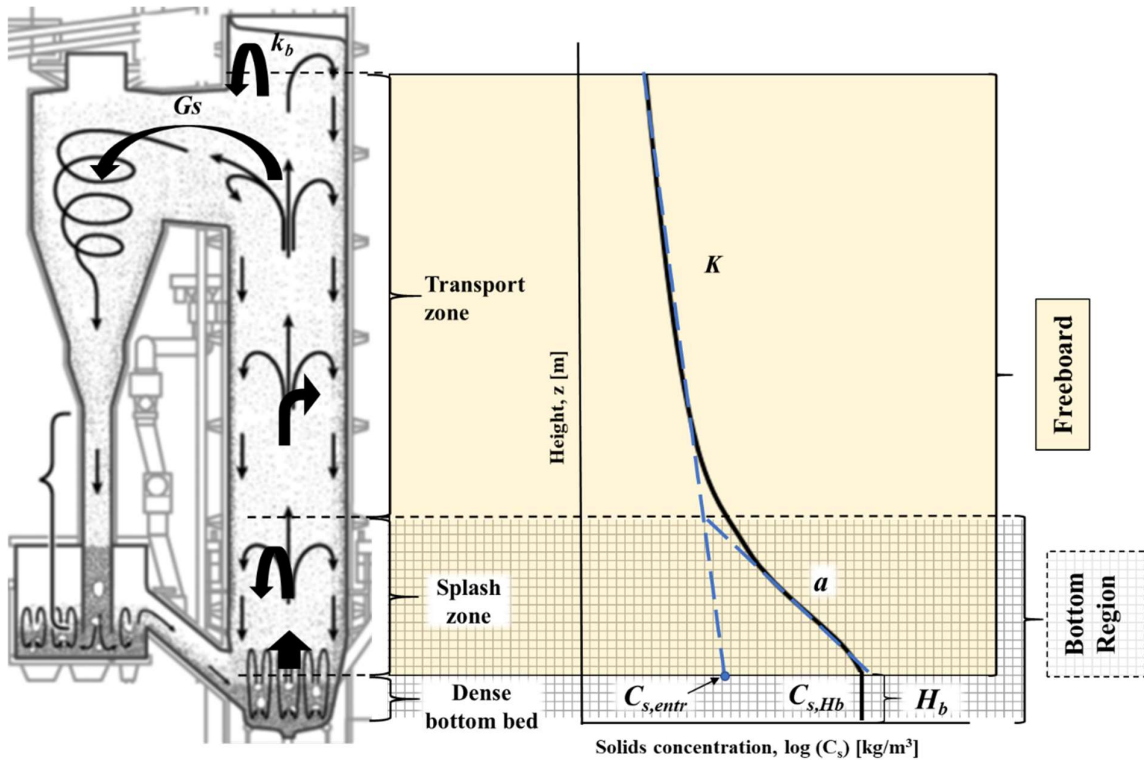
Figure 3. Fluid-dynamical regions in the furnace of a CFB boiler according to Johnsson and Leckner [17], indicating the key parameters in the vertical profile of solids concentration used in Eq. (9).

The external circulation of solids is often estimated to be equal to the solids up-flow at the riser top [17, 18, 40, 48, 49] (F_{top} in Figure 2). However, studies have shown that there can be significant solids back-mixing at the riser exit, as the gas is not able to drag all the solids into the cyclone duct [38, 40, 50-52]. This phenomenon – known as the *back-flow effect* – has been shown to depend on the geometry of the exit region [32, 50, 51], as well as the local particle size and concentration [38] ($F_{backflow}$ in Figure 2). The back-flow ratio, k_b, is defined as:

$$k_b = \left. \frac{G_{s,layer}}{G_{s,core}} \right|_{h=H} \tag{10}$$

Therefore, the external circulation of solids in a CFB boiler is the end result of a sequence of fluid-dynamical mechanisms that involve entrainment from the bottom region, back-mixing in the transport zone, and back-flow in the exit region. These phenomena (characterized by the terms $C_{s,entr}$, K and k_b, respectively) can be aggregated to yield the externally circulating solids flux, G_s (see F_s in Figure 2) (under the assumption that the dispersed solids flow according to their single particle terminal velocities):

$$G_s = \underbrace{\underbrace{C_{s,entr}\left(u_g - u_t\right)}_{\text{entrained from bottom region}} e^{-K(H-H_b)}}_{\text{yielding furnace top}} (1 - k_b) \tag{11}$$

Measurement of the external circulation of solids in large-scale units is a major challenge. Only a few values have been published in the literature [18, 23, 48, 49, 53], and some of these lack a clear description of how they were derived. For this, a consistent, well-documented method is to solve the heat balance over a loop seal system equipped with a heat exchanger [49]. In addition, care should be taken when comparing values for the external solids circulation obtained from different units, since several unit-specific variables (e.g., riser height, cross-sectional dimensions, secondary air location, and the inclination of tapered walls) are known to influence the external solids circulation.

2.2 Closure of the mass balance

The solids flow in the furnace is typically studied indirectly through the vertical profile of the solids concentration [Eq. (9)], since the latter is relatively straight-forward to obtain from pressure drop measurements along the height of the furnace. Neglecting acceleration effects, a measured pressure drop between two heights can be recalculated into an average solids concentration for the height interval. First, the voidage (ε) is solved from the general expression for the pressure drop:

$$\Delta P = \left(\rho_s\left(1 - \varepsilon_g\right) + \rho_g \varepsilon_g\right)g\Delta h \tag{12}$$

Thereafter, the solids concentration can be calculated as:

$$C_s = \rho_s\left(1 - \varepsilon_g\right) \tag{13}$$

Due to the limited number of pressure measurements in large-scale CFB furnaces, there will, as mentioned above, be poor spatial resolution in the vertical pressure drop profile and, since the bottom-most pressure measurement is typically located at some significant height above the nozzle level, some uncertainty related to the total pressure drop in the riser, ΔP_{riser}.

The reason for the limited number of pressure measurements is that usually only the overall pressure drops in the upper half and lower half of the furnace are used as control parameters for the operation of the boiler and to determine the charging/discharging of the bed material. Thus, the riser pressure drop is typically an operational input to models of CFB boilers, together with the air feeding. Other given inputs to the modeling are the geometry of the unit and the density of the bed solids. The particle size distribution of the solids inventory contained in the loop is complicated to evaluate due to the solids attrition and the size segregation effects in the fluid-dynamics of the bed and in the cyclone separation and bottom bed discharges [54]. While advanced semi-empirical models for CFB combustion include population balances for the bed solids, to solve the size distribution of the solids inventory established in the unit, many simpler models and CFD simulations disregard this aspect and assume that the solids inventory in the unit is known. For simplicity and focus, the discussion in this section assumes that solids size is a known input.

Figure 4 illustrates the closure of the solids mass balance in the furnace, i.e., the determination of the vertical profile of the solids concentration, from the above-given inputs and expressions. Determination of the solids concentration profile [Eq. (9)] requires the calculation of five unknowns: H_b, C_{s,H_b}, $C_{s,entr}$, a, and K. An additional equation for system closure is provided by the calculation of the riser pressure drop from the spatial integration of the solids concentration profile [Eq. (9)]. Assuming that $C_s = \rho_s\left(1 - \varepsilon_g\right) \gg \rho_g \varepsilon_g$ [see Eq. (12)], the following expression is obtained:

$$\Delta P_{Riser} = C_{s,H_b}gH_b + \frac{\left(C_{s,H_b} - C_{s,entr}\right)g}{a}\left(1 - e^{-a(H-H_b)}\right) + \frac{C_{s,entr}g}{K}\left(1 - e^{-K(H-H_b)}\right)$$

$$\tag{14}$$

As schematized in Figure 4, Eq. (14) is typically used to calculate the dense bed height. Thus, four parameters, C_{s,H_b}, $C_{s,entr}$, a, and K, need to be calculated for determination of the solids concentration profile. The literature provides expressions (most of them purely empirical) for all these parameters, with the exception of $C_{s,entr}$ [8, 17, 33, 38, 39], as summarized below.
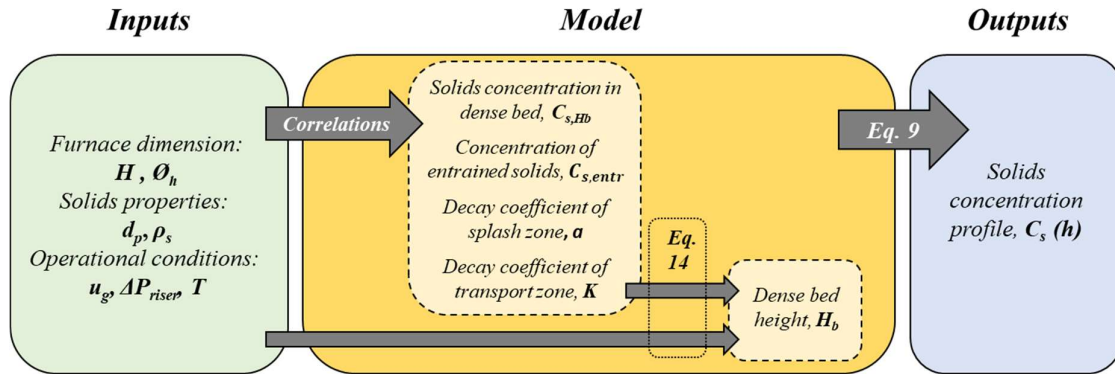
Figure 4. Schematic overview of the system for predicting the solids concentration profile

The solids concentration in the dense bottom bed can be approximated through interpolation/extrapolation of the experimental data (see [36] for the measured values in the bottom bed of the 12-MW$_{th}$ Chalmers boiler for two different particle sizes) or calculated by means of semi-empirical expressions based on the modeling of the gas flow [38].

The exponential coefficient, *a*, which characterizes the vertical decay of the solids concentration in the splash zone, was in laboratory-scale CFB units observed by Kunni and Levenspiel [39] to follow the trend:

$$au_g \approx constant \tag{15}$$

Based on the data from runs with three different particle sizes in the Chalmers 12-MW$_{th}$ CFB boiler, Johnsson and Leckner (1995) [17] have proposed:

$$a = 4\frac{u_t}{u_g} \tag{16}$$

An empirical correlation for the decay coefficient in the transport zone, *K*, describing the solids back-mixing to the wall layers was proposed by Johnsson and Leckner [17] based on measurements from the 12-MW$_{th}$ Chalmers boiler (covering the region u_g-$u_t \leq 3$) and three larger units (covering the region u_g-$u_t \geq 4.5$):

$$K = \frac{0.23}{u_g - u_t} \tag{17}$$

It should be pointed out that there was a significant scatter in the data and that the larger boilers yielded lower values of K than did the Chalmers boiler. This is in line with the work of Johansson et al. [40], which concluded that Eq. (17) could not generally describe large-scale CFB boilers and instead proposed an expression based exclusively on the geometry of the furnace:

$$K = \frac{1}{H} \tag{18}$$

In summary, calculation of the parameters that define the solids flow in large-scale CFB furnaces relies on empirical correlations derived from limited sets of measured data (often unit-specific and sometimes without any resemblance to large-scale conditions). Moreover, the solids entrainment from the bottom region has not been investigated for conditions relevant to large-scale CFB boilers. Therefore, expressions that have a more-solid theoretical basis and that are validated for a wide range of sizes and operational conditions are needed to yield a more robust prediction of the solids flow.

2.3   Fluid-dynamical scaling

Fluid-dynamical scaling, which is used in many different applications, facilitates studies of the fluid dynamics of challenging environments (e.g., large-scale, industrial environments, high-temperature conditions) in smaller laboratory-scale units operated under ambient conditions, without losing the quantitative relevance of the measured data. Fluid-dynamical scaling also allows for the use of diagnostic techniques that are not suitable for harsh environments. It is based on the reformulation of continuity and momentum balances into their dimensionless forms and, therefrom, extraction of the dimensionless parameters that need to be held constant in order to maintain the similarity between the reference unit and the laboratory unit. Table 1 shows the collected scaling parameters for the different scaling sets discussed below, together with their respective positive and negative aspects.

Table 1 lists different sets of fluid-dynamical scaling laws. Glicksman [55] has proposed a full set of scaling parameters for an FB (used, for example, in [56, 57]), in which the length scale factor, L^*, is given by the gas chosen for operation of the cold-flow model:

$$\frac{u_0^2}{gD}, \frac{\rho_s}{\rho_g}, \frac{\rho_s u_0 d_p}{\mu_g}, \frac{\rho_g u_0 L}{\mu_g}, \frac{L}{D}, \frac{G_s}{\rho_s u_0}, \emptyset, PSD \tag{19}$$

$$L^* = \frac{L_{cold}}{L_{ho}} = \left(\frac{\mu_g}{\rho_g}\bigg]_{cold} \bigg/ \frac{\mu_g}{\rho_g}\bigg]_{hot} \right)^{2/3} \tag{20}$$

When applied to the down-scaling of a CFB combustor (operating at approximately 850°C), a cold-flow model fluidized with ambient air [Eq. (20)] yields a length scale factor of approximately L^*=0.2. Note that for utility-scale CFB boilers (with furnace heights typically up to 40 m), this would imply air-blown cold-flow models of considerable dimensions (8 m in height).

Both Horio et al. [58] and Glicksman et al. [59] have presented simplified scaling laws, given in rows 3 and 2, respectively, of Table 1, where Glickman's simplified set of scaling reads:

$$\frac{u_0^2}{gD}, \frac{\rho_s}{\rho_g}, \frac{u_0}{u_{mf}}, \frac{L}{D}, \frac{G_s}{\rho_s u_0}, \emptyset, PSD \tag{21}$$

The set of scaling laws presented by Horio and colleagues is similar, with u_t substituting for u_{mf} in the third dimensionless group [60]. This results in only minor variations of the resulting scaling.

The simplified set of scaling laws results in a length scale factor of:

$$L^* = \frac{L_{cold}}{L_{hot}} = \left(\frac{u_{mf}]_{cold}}{u_{mf}]_{hot}} \right)^2 \tag{22}$$

This length scale factor can be adjusted by varying the particle size [note that the solids density is given by the second dimensionless group in Eq. (19) or Eq. (21)], resulting in finer solids yielding smaller cold-flow models. It should also be noted that for finer solids, other forces, such as inter-particle forces and static charging, may also affect the solids flow.

Therefore, it is crucial to keep the scaled solids in the same Geldart Group as the reference solids. The flexibility offered by the simplified set in designing cold-flow models has meant that it has evolved into a widely used tool in the field of fluidization (see, for example, [32, 51, 59-63]). The validity of this simplified set of scaling laws is proven at both low and high particle Reynolds numbers, i.e., it is assumed to be generally valid.

Table 1. Sets of fluid-dynamical scaling laws and their negative and positive aspects.

Sets of fluid-dynamical scaling									Negative aspects	Positive aspects
Glicksman full set	$\frac{u_0^2}{gD}$	$\frac{\rho_s}{\rho_g}$	$\frac{\rho_s u_0 d_p}{\mu_g}$	$\frac{\rho_g u_0 L}{\mu_g}$	$\frac{L}{D}$	$\frac{G_s}{\rho_s u_0}$	$\emptyset$	PSD	Fixed-length scale factor. Yields fine, heavy particles in small units, and thus potentially strong inter-particle forces.	The fluid dynamics are fully scaled
Glicksman simplified set	$\frac{u_0^2}{gD}$	$\frac{\rho_s}{\rho_g}$	$\frac{u_0}{u_{mf}}$		$\frac{L}{D}$	$\frac{G_s}{\rho_s u_0}$	$\emptyset$	PSD	Yields fine, heavy particles in small units, and thus potentially strong inter-particle forces. Is associated with substantial challenges, e.g., hazardous properties.	Adjustable length scale factor. Validated for high and low particle Reynolds numbers.
Horio simplified set	$\frac{u_0^2}{gD}$	$\frac{\rho_s}{\rho_g}$	$\frac{u_0}{u_t}$		-	$\frac{G_s}{\rho_s u_0}$	-	-		
Van der Meer et al. simplified set	$\frac{u_0^2}{gD}$	-	$\frac{u_0}{u_t}$		$\frac{L}{D}$	$\frac{G_s}{\rho_s u_0}$	-	-	Loss of quantitative value for pressures/solids concentrations. Validated only for a viscous regime.	Adjustable length scale factor and solids type

Hazardous material and environmental issues arise with the use of very small and heavy particles. Van der Meer et al. [60] have proposed a further simplification of the scaling sets (see row 4 in Table 1), whereby the $\frac{\rho_s}{\rho_g}$ parameter is omitted [60], providing the opportunity to choose the particles more freely. This has been validated experimentally by Glicksman for very low Reynolds numbers [15]. Van der Meer et al. [60] have noted that this simplified scaling maintains only approximately the fluidization regime and macroscopic movement of the solids. The mass and pressure drop similarities are lost, while the riser solids volumetric hold-up is more or less maintained [60].

In contrast to other CFB systems (e.g., fluid catalytic cracking), the external solids circulation in CFB boilers is neither an externally controllable nor a known parameter. Rather, it is a consequence of the riser design and operation. Instead, the riser pressure drop is used as a known control parameter in CFB boilers. Thus, the dimensionless group $\frac{G_s}{\rho_s u_0}$ is replaced in the scaling of CFB boilers with the dimensionless riser pressure drop, $\Delta P/\rho_s gL$, which is accounted for to ensure the similarity of the solids flows.

CHAPTER 3
Experimental work

3.1   **Experimental setup**

In the present work, two experimental units were used: a pseudo-2-dimensional (pseudo-2D) unit, and the above-mentioned cold-flow scale model of a >200-MW$_{th}$ CFB boiler, which were operated with and without scaled bed material. Table 2 shows the main dimensions and operational parameters for the three experimental setups used in this work, and the papers to which they contribute data.

The overall experimental setup is similar for all the cases: the fluidizing air is fed by two inlet fans coupled in series and controlled with flowmeters and valves through a LabView interface. Pressurized air is used for the auxiliary systems, such as those controlling fluidization of the particle seal and purging of the pressure sampling lines. The air distributor plates provide a pressure drop, which is chosen so as to be similar to those applied in industrial boilers. This is necessary to ensure the same bottom bed regime [36] as is used in industrial units. A cyclone separates the externally circulating particles from the air flow, and a particle seal ensures recirculation of the solids into the riser without any bypass of gas up through the cyclone. The concentration of solids in the riser is assessed through pressure drop measurements, and the rate of solids circulation is estimated using a butterfly valve with an in-built air plenum that is placed in the cyclone leg. The different solids used in the papers all belong to Geldart Group B.

Table 2. Experimental setups used in this work. Upscaled values for the scaled tests are given in italics in parentheses.

			Pseudo-2D unit	*Cold-3D unit* (non-scaled material)		*Fluid-dynamical scaled tests* (scaled material)
			Papers I, IV	*Papers II, IV*	*Paper IV*	*Papers III, IV, V*
Cross-sectional area	$D \times W$	m^2	0.7×0.12	0.45[*]	0.45[*]	0.45[*] *(75)*[*]
Height	H	m	8.5	3.1	3.1	3.1 *(40)*
Particle diameter	d_p	μm	316	112	122	35 *(195)*
Particle density	ρ_s	kg/m^3	2,600	2,600	3,950	8920 *(2,480)*
Minimum fluidization velocity	u_{mf}	m/s	0.067	0.013	0.019	0.0045 *(0.0162)*
Terminal velocity	u_t	m/s	2.21	0.64	1.29	0.28 *(1.01)*
Fluidization velocity	u_0	m/s	[0.3–7.0]	[0–1.4]	[2.2–2.6]	[0.17–1.25] *([0.6–4.5])*
Riser pressure drop	ΔP_{Riser}	kPa	[1.7–10.5]	[0.15–3.50]		[0.9–2.3] *([3.2–8.4])*

[*] The dimensions of the furnace walls are not disclosed for reasons of confidentiality.

3.1.1. Pseudo-2-dimensional unit

Figure 5 shows the bottom part of the pseudo-2D unit with the dimensions (D×W×H) of the riser being 0.7×0.12×8.5 m^3 (for further details, see Table 2). The riser depth of 0.12 m and the bed material used (glass beads) explain why no wall effects were observed along the wide dimension (i.e., through the front side, which is made of Perspex) in the bottom part of the riser. In the upper region (transport zone), a flat solids flux profile along this wide dimension was observed, whereas the narrow dimension was shown to give a parabolic solids flux profile, similar to those seen in small and narrow risers with a circular cross-section [64]. In summary, the unit enables visualization of the qualitative solids flow established in a vertical slice of a CFB boiler and this, therefore, is characterized as a *pseudo-2D* unit. The unit also has sufficient height to allow for a fully developed transport zone. The 24 pressure measurement points are densely spaced in the bottom of the riser, with 11 taps located within the first meter above the grid.

Figure 5. Bottom part of the pseudo-2D unit.

3.1.2.   Fluid-dynamically down-scaled unit

In the present work, a reference >200-MW$_{th}$ CFB boiler is fluid-dynamically down-scaled (the exact boiler capacity cannot be disclosed because the reference boiler is a commercial boiler). The reference boiler has a cross-sectional area of 75 m^2 and a height of 40 m, and is operated at 850°C with a bed material that consists primarily of make-up material (silica sand), with a mean particle diameter of 190 μm and a density of 2,600 kg/m^3.

Using Glicksman's full set of scaling laws [Eq. (19)] and ambient air as the fluidization medium in the cold-scale model, the resulting scaling factor is L^*=1/4.4=0.23. This would result in the cold-scale model having a height of 9.5 m and a cross-sectional area of 4.3 m^2, requiring a ceiling height and air feeding capacity beyond what would be economically feasible for the laboratory facilities used in this work. This case is marked in gray in Table 3, and would have been the optimal scaling scenario. Instead, the simplified scaling laws (*cf.* Table 1) were applied, which gave the values of the dimensionless groups listed in the last column of Table 3.

Table 3. Fluid-dynamical scaling discussed in this work applied to the >200-MW$_{th}$ reference CFB boiler. Up-scaled values for the corresponding boiler are given in italics in parentheses.

			Reference Boiler	Glicksman's full set *(not applied in this work)*	Glicksman's simplified set *(applied in Papers III, IV, V)*
Cross-sectional area	$D{\times}W$	m^2	75	4.3 *(75)*	0.445 *(75)*
Height	H	m	40	**9.5** *(40)*	3.1 *(40)*
Gas density	ρ_g	kg/m^3	0.33	1.2 *(0.33)*	1.2 *(0.33)*
Gas viscosity	μ_g	Pas	$4.3{*}10^{-5}$	$1.8{*}10^{-5}$ *($4.3{*}10^{-5}$)*	$1.8{*}10^{-5}$ *($23{*}10^{-5}$)*
Particle diameter	d_p	μm	190	**45** *(190)*	35 *(194)*
Particle density	ρ_s	kg/m^3	2,600	**9,397** *(2,600)*	8,920 *(2,468)*
Minimum fluidization velocity	u_{mf}	m/s	0.0155	0.0076 *(0.0155)*	0.0043 *(0.0155)*
Terminal velocity	u_t	m/s	0.95	0.46 *(0.96)*	0.28 *(1.01)*
Dimensional scaling factors					
Length	$L^* = L_{Cold}/L_{Hot}$ $= \left(u_{mf_{Cold}}/u_{mf_{Hot}}\right)^2$			0.23	0.077
Time	$t^* = t_{Cold}/t_{Hot}$ $= \left(u_{0_{Cold}}/u_{0_{Hot}}\right)^2$			0.48	0.28
Mass	$m^* = m_{Cold}/m_{Hot}$ $= \rho_{g_{Cold}}/\rho_{g_{Hot}} * (L_{Cold}/L_{Hot})^3$			0.0442	0.0016

Applying Glicksman's simplified set of scaling laws, a scale model that operates with ambient air can be designed that offers a somewhat adjustable scaling (see Section 2.3) through the choice of solids. A good compromise was adjudged to be a length scale factor of 1/13, which requires solids that yield a minimum fluidization velocity of 0.0043 m/s [Eq. (22)] in the cold-scale model. The optimal solids density (9,397 kg/m^3) is given by the density ratio, although materials with this density present substantial challenges in that they can be hazardous materials (lead mixtures), hazardous due to the fine sizes required (30–50 μm), radioactive (polonium) or very expensive (gold, silver).

As a consequence, copper (8,920 kg/m^3) was chosen as the bed material for the cold-scale model. With the solids density fixed, the solids size is the parameter through which the minimum fluidization velocity (and, thereby, the length scale factor) can be adjusted. The design values for the cold-scale model (L*=1/13=0.077 and, thereby, u_{mf}=0.0043 m/s) could be attained with a particle diameter of 35 μm, which assigns the particles to the Geldart Group B solids. With this, a cold-scale model resembling the reference boiler with a scale factor of 1/13 was designed and built according to Glicksman's simplified set of scaling laws, using the scaling parameters listed in Table 3. For the scale model used, the corresponding up-scaled values are given in parentheses in the Table 3, indicating the error incurred when the exact values derived from the scaling laws cannot be applied in practice. For example, the copper solids employed are lighter than the specification, and they scale up to a value of 2,468 kg/m^3 rather than the density of the material in the reference boiler (2,600 kg/m^3).

The cold-scale model and associated instrumentation used in this work are depicted in Figure 6 and in a 3D depiction of the cold-scale model in Figure 7. For this setup, a suction fan and a filter were installed downstream, to ensure that the bed pressure was maintained below atmospheric pressure (thus avoiding potential leakage of the bed material) and to allow control of the atmospheric-pressure height in the riser, in a manner similar to that in commercial CFB boilers.
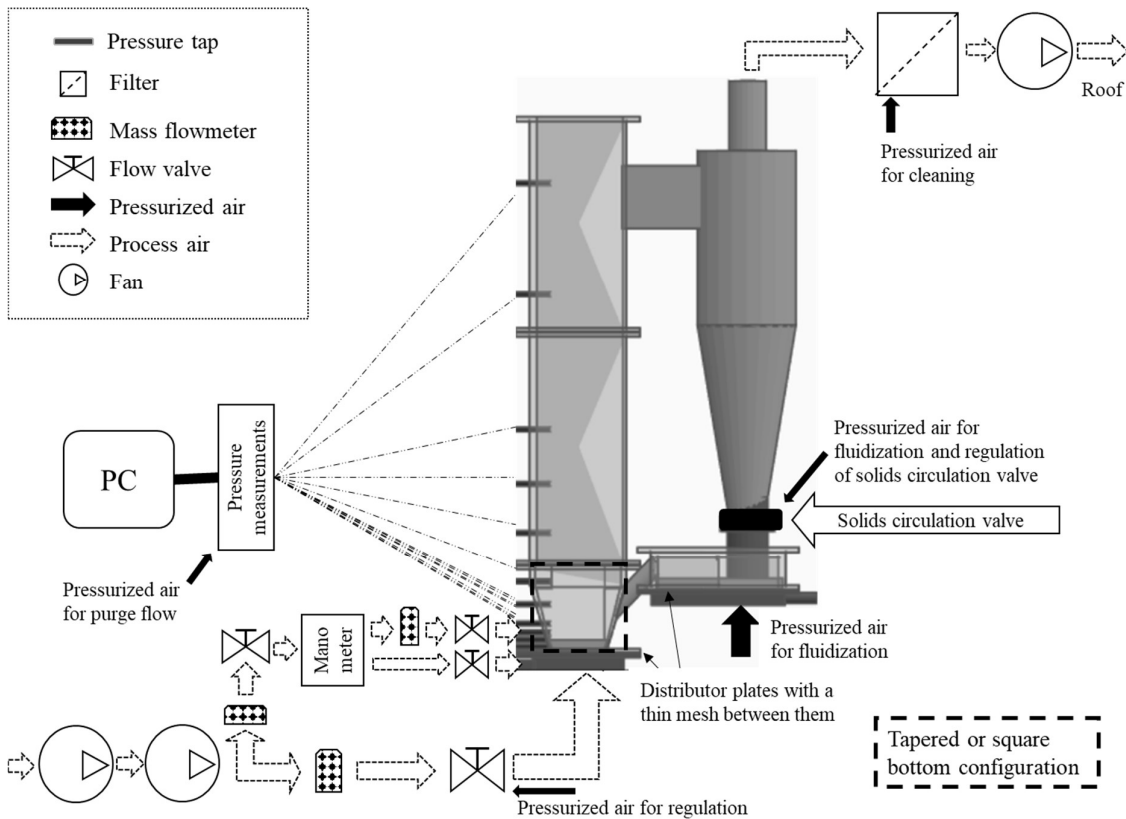
Figure 6. Schematic of the cold-scale model and its instrumentation. Source: Paper III.

The riser of the unit is equipped with 15 pressure transducers. As mentioned previously, this is in strong contrast to the pressure data collection systems used in commercial boilers, in which only a few (typically, 3–6) transducers are placed in the riser, yielding a much lower spatial resolution of the solids concentration profile. An even higher spatial resolution would be desirable in the lower part of the riser of the cold-scale model. However, due to scaling, the pressure differences between the measuring ports becomes very small for some cases (e.g., in cases of low solids inventories or operation with a high fluidization velocity) and the measuring error of the pressure transducers becomes significant. Nonetheless, the 15 pressure transducers used provide finer resolution than that obtained in a typical commercial boiler.

Two different bottom configurations were used. Tapered walls were used to resemble the riser geometry of the reference boiler in the scaling validation cases described in **Paper III**, while vertical bottom walls were used for further measurements. The different bottom configurations (vertical/tapered walls) are compared in **Paper IV** in terms of the solids entrainment from the bottom region into the transport zone**.** The unit has lateral air injection points at three different heights, which are used for the injection of recirculated flue gas and secondary and tertiary air streams. The cyclone is not scaled but is modeled to ensure that the bed material is retained within the circulation loop. This requires a slightly modified shape of the loop seal, which is designed to contain the same volume of solids as in the reference boiler.
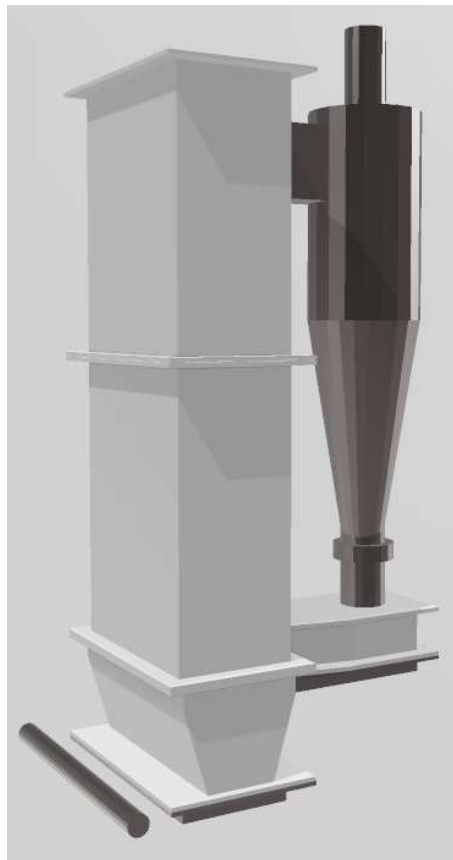
Figure 7. 3D depiction of the cold-scale model.

Figure 8. Photographs of the cold-scale model with: a) non-scaled particles (glass particles); and b) scaled particles (copper).

The cold-scale model was used for the experiments in **Papers II–V**, as described in Table 2 and depicted in Figure 7. The unit is down-scaled with Glicksman's simplified scaling laws (see Section 2.3). Silica glass particles that did not fulfill the Glicksman's scaling laws were used for **Papers II** and **IV** (Figure 8a), and copper particles that fulfilled Glicksman's scaling laws were used in **Papers III–V** (Figure 8b).

Validation of the cold-scale model was performed on the basis of comparisons to the measurements made in the reference >200-MW$_{th}$ CFB boiler for four cases representative of different operational states (see Figure 9). Measurement data from the reference boiler consist of time-averaged pressure values collected over a period of 81–300 minutes with a logging frequency of 0.1 Hz. From these pressure measurements, the solids concentration profiles were derived through Eq. (12). The cases considered had loads that ranged from 60% to 100% and solids concentrations at the top of the furnace that ranged from 0.4 to 3.0 kg/m^3. The comparison of the particle concentration profiles shows good agreement for all four reference cases (Figure 9), so the scaling is considered to be successfully validated.

25
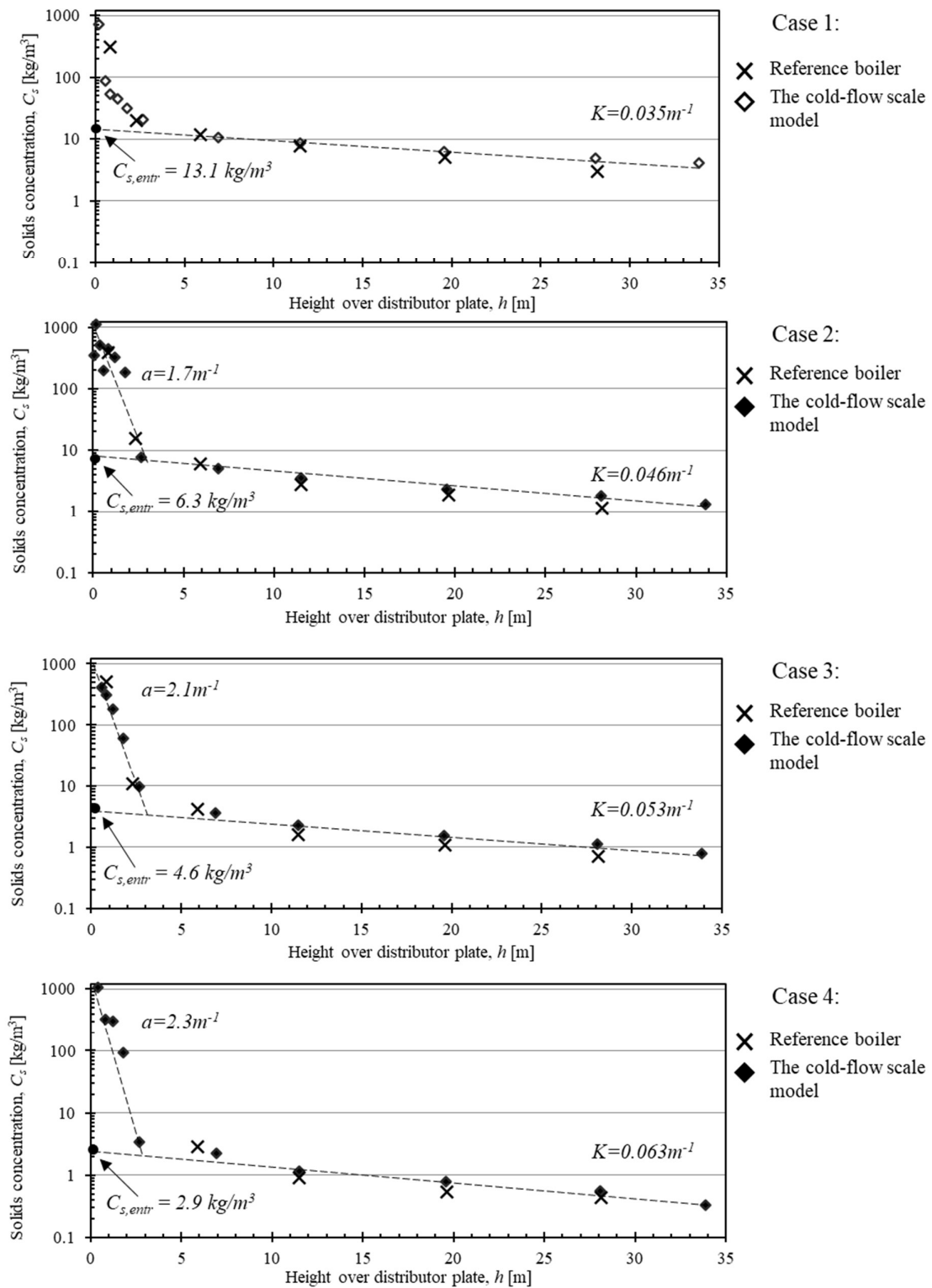
Figure 9. Comparisons of the solids concentration profiles between the reference >200-MW$_{th}$ CFB boiler and the corresponding cold-scale model for four cases representing different operational states. Source: Paper III.

3.2 Processing of measurements

The high number of pressure transducers along the risers of the units used in this work allows for determination with relatively high spatial resolution of the vertical profile of the particle concentration. The distance between pressure transducers varies along the riser, being shortest in the bottom region (in the order of 0.5–1.0 cm) and longest at the top (up to 50–100 cm, depending on the unit). Thus, this work provides data with uniquely high resolution for the bottom region. From the measurements made in the bottom region, the following three categories are established in terms of the presence or absence of a dense bed (summarized in Table 4):

- **Presence of a dense bed**. The pressure measurements show a linear decrease with the height of the riser. To assess this, a minimum of three pressure measurements within the dense bed is needed [36]. Note that a typical dense bed height for CFB boilers is reported in the literature as 0.4–0.6 m, and it decreases with the fluidization velocity [36].
- **Uncertain presence of a dense bed**. Although a linear pressure decrease is not observed, a dense bed that is lower than the height of the third pressure tap could still be present, since a solids concentration >750 kg/m^3 (implying that the emulsion phase occupies a larger volume than the bubble phase) is noted.
- **Absence of a dense bed**. Neither a linear pressure drop nor a dominant emulsion phase is observed.

The symbols listed in Table 4 are used in all the papers to indicate to which of the above-mentioned categories the bottom region belongs.

Table 4. Criteria used to categorize the experimental runs in terms of
the fluid dynamics in the bottom region. Source: Paper III.

Category	Dense bed present?	Symbol		*Criterion 1:* Linear pressure drop across three lowest bottom measurements	*Criterion 2:* bubble fraction <0.5
1.	yes	■	Filled	yes	yes
2.	unclear	⊟	Half-filled	no	yes
3.	no	□	Not filled	no	no

The external solids circulation is measured with a butterfly valve (Figure 10). Once this valve is closed, it fluidizes the material accumulating above it in the downcomer. The rate of circulation of solids is calculated from the rate of the pressure increase, as illustrated in Figure 10.
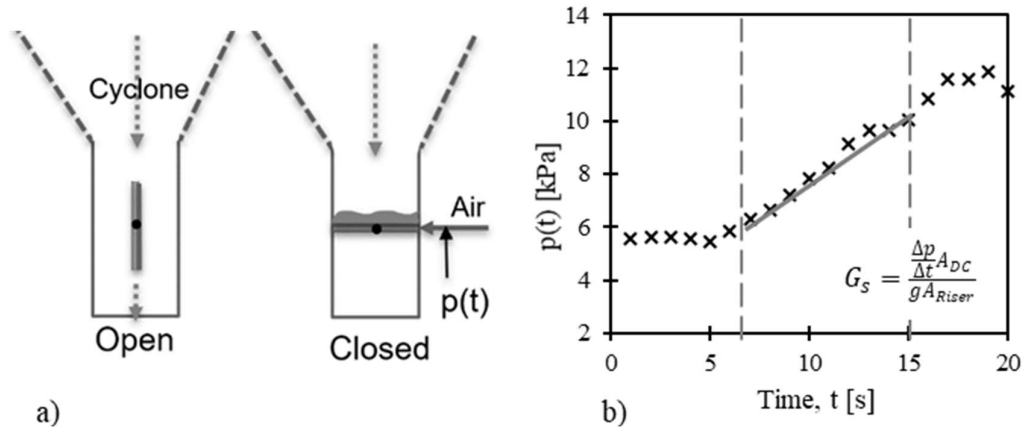
Figure 10. Measurement of the external solids circulation. a) Schematic showing the functionality of the butterfly valve in the downcomer. b) Transient pressure increase and corresponding solids circulation. Source: Paper III.

To maximize the validity range of the findings and proposed expressions, this work makes use of all the data from large-scale CFB boilers available in the literature (to the best of the knowledge of the author). Information from the 10 units considered and the cases reported is given in Table 5.

Table 5. Gathered data from the literature used in this work [17, 18, 20-25, 65], together with their plotting markers. Numbers indicated in red are approximated values. Source: Paper V.

Name	Capacity	D [m]	W [m]	Øh [m]	H [m]	ug [m/s]	dp [mm]	ut [m/s]	Cs,min [kg/m³]	Cs,max [kg/m³]
Chalmers [17]	✳ 12-MWth	1.6	1.4	1.5	13.5	[2.7, 4.7]	0.2, 0.32	[1, 2.1]	2.6	40
Flensburg [18]	✚ 109-MWth	5.13	5.13	5.1	28	6.3	0.2	1.0	3	17
Huchet [21]	▲ 125-MWe	12.8	4.3	6.4	33	[4.8, 3.6]	0.25	1.5	1.6	36.6
Örebro [20]	★ 165-MWth	12	4.7	6.8	33.5	4.6	0.27	1.7	1.7	5
Duisburg [18]	● 105-MWe	Diam	8	8	32	5.3	0.17	0.8	5.1	20.5
Ref Boiler [65]	◆ >200-MWth	75 m²		8.4	40	[3.5, 2.7, 2.2, 1.5]	0.19	1.1	0.5	12
Cold-scale model [65]	◇ >200-MWth	75 m²		8.4	40	[0.6-4.5]	0.195	1.1	0.1	25
Zibo [25]	◉ 135-MWe	13.1	6.6	8.8	38	[3.9, 4.0, 2.9]	0.17	0.8	2.5	64
Gardanne [22]	♥ 250-MWe	11.5	14.8	12.9	>36	5.2	0.3	1.9	3.2	16
Turow [23]	⚕ 235-MWth	21.1	9.9	13.5	44	5.3	0.3	1.9	3.1	18.8
Lagisza [24]	■ 460-MWe	10.6	27.6	15.3	48	[3.9, 3.0, 2.1, 1.6]	0.22	1.2	1.5	90

Experimental data gathered from the literature on commercial-scale CFB boilers are given in the form of vertical profiles of either pressure or solids concentration. Calculating the decay coefficient of the transport zone, K, and the entrained solids concentration, $C_{s,entr}$, from these data is often challenging given the limited number of pressure taps available in commercial CFB boilers and the need to select those data-points that belong to the transport zone (and not affected by top and exit furnace configuration). For an example of this see Figure 11, where the consideration of different sets of data-points yields strongly differing values for the decay coefficient.

This work takes the average value for the calculations. However, it considers the maximum and minimum values obtained, so as to gauge the level of uncertainty in the evaluation. Obviously, a higher spatial resolution of the upper part of the furnace results in a smaller degree of uncertainty in the calculation of the decay coefficient.
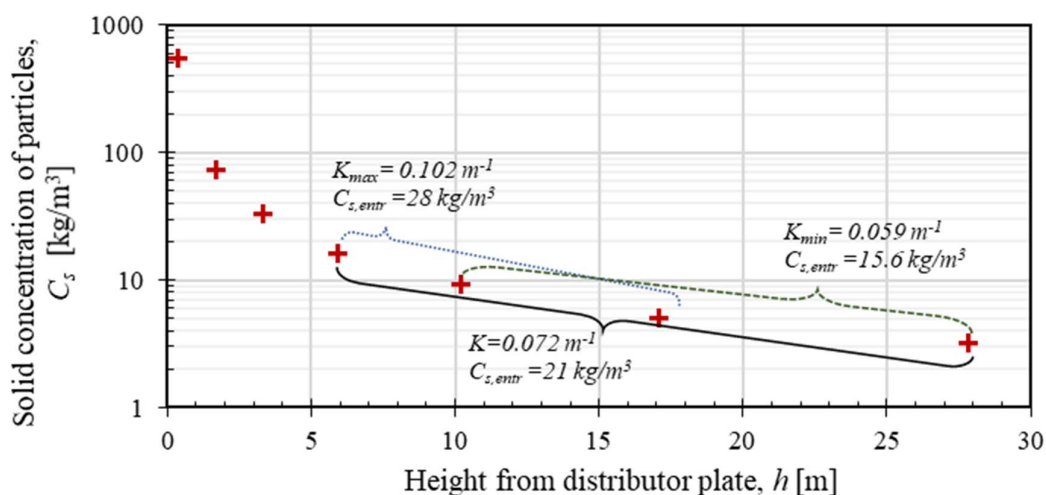
Figure 11. Experimental solids concentration data from the Gardanne 250-MW$_e$ CFB unit [22]. The brackets illustrate how different datasets influence the values of the parameters extracted. Compiled from Paper V.

CHAPTER 4
Modeling

This work adopts several modeling approaches, each providing different value for the investigations. Below, short descriptions are given of the types of models employed and the goals associated with their use.

4.1 Monte Carlo modeling of trajectories of solids clusters

As a method, Monte Carlo modeling is based on the simulation of a number of events, in a system that is governed by parameters that are described by a probability distribution. The results can then be used to generate a statistically robust solution, without the need for a solver.

In this work, Monte Carlo modeling is used for evaluating whether the vertical distribution of solids clusters ejected into the splash zone can be derived using the hypothesis that they follow a ballistic trajectory solely driven by gravity. The model applies probability distributions for the angle and velocity of the solids ejections taken from experimental work in literature [66, 67]. The statistical vertical profiles of the solids concentrations obtained from the Monte Carlo simulations are compared to the exponential decays measured experimentally. It is concluded that the expressions described in the literature for the velocity and angle of ejection combined with the assumption of a ballistic trajectory yield back-mixing rates that are in agreement with the experimental observations. This is discussed in greater detail in **Paper IV**.

4.2 FVM modeling of the mass balance for the solids phase

The finite volume method (FVM) is used to discretize the transport equation that represents the mass balance for the solids, when considered as a continuous phase.

The model is in this work applied to solve the steady state of the solids disperse phase in the core region of the transport zone, which is discretized in the three spatial dimensions. Both convective transport and dispersive transport are considered in the balance, as well as source terms – all of these expressed through semi-empirical expressions, since the momentum balance is not considered so as to ensure affordable calculation costs.

With the help of the model, it is shown that the lateral dispersion of solids in the core region is much faster than the core-to-layer transport, and the general validity for larger-scale CFB furnaces of some of the expressions in the literature describing the lateral dispersion coefficient is discarded (see **Paper V** for details).

4.3 DNS modeling of solids particles

Direct Numeric Simulation (DNS) solves the Navier Stokes equation, resolving all time scales and length scales, from microscales to macroscales, in the continuous gas phase and tracking each solid particle as a discrete element through the equation of motion. DNS provides a highly resolved and reliable simulated flow for the given boundary conditions, although it comes at a very high computational cost, which limits the domain volume and number of particles that can be studied.

This work uses DNS in **Paper V** to gain insights into the solids core-to-layer transfer under conditions representative of the transport zone in large-scale CFB furnaces. The trajectories of the considered solid particles provide statistical information about the dynamics of the solids concentration and velocity fields. This allows the identification of turbophoresis, which is the phenomenon whereby particles in a gas migrate in the direction of decreasing turbulence level, as the governing factor for the lateral flow of core-region-solids in the vicinity of the wall layer. This phenomenon is superimposed onto the macroscopic dispersive solids movement from high- to low-concentration regions. In CFB furnaces, this translates into that the particles in the core region (on average) move towards the wall layer region with lower velocity fluctuations than in the core region [68-70]. The finding that turbophoresis is the driving force for the core-to-layer solids transfer validates the use of field-specific expressions for parameters such as the deposition velocity to study and correlate the solids back-mixing in the transport zones of commercial CFB furnaces.

CHAPTER 5
Results and Discussion

This chapter provides a summary of the work included in **Papers I–V** and discusses how the findings and expressions derived from the studies can be used for closure of the solids mass balance in large-scale CFB furnaces. A short schematic summary of the main findings related to the key mechanisms for the solids flow patterns in the large-scale CFB furnace is presented in Figure 12.

The particle size segregation with height in the furnace influences the terminal velocity of the solids and, thereby, the velocity at which the solids flow. At a low fluidization velocity, only the smallest particles will be entrained, yielding a strong size segregation effect between the particles populating the top of the furnace and circulating in the system and those remaining at the bottom of the furnace. As the fluidization velocity is increased, coarser solids will be entrained and, thus, the vertical size segregation will decrease. For the scaled experiments, the extent of this size segregation effect (between circulating particles and those remaining at the bottom of the furnace) is shown in Table 6. This table lists the distributions of sizes and single particle terminal velocities for solids samples from one case in the riser and the loop seal (sampled after defluidization) at different fluidization velocities. The particle size distribution of the solids in the riser is approximately constant for all the cases, as it holds a large share of the solids mass in the system. The average particle size in the loop seal increases with fluidization velocity and approaches that in the riser as the fluidization velocity is increased.

Table 6. Distributions of the solids sizes and single particle terminal velocities in the down-scaled model representing a >200-MW$_{th}$ CFB boiler (up-scaled values). Source: Paper III.

	d_{p10} (μm)	d_{p50} (μm)	d_{p90} (μm)	$u_t(d_{p10})$ (m/s)	$u_t(d_{p50})$ (m/s)	$u_t(d_{p90})$ (m/s)
Riser	106	**195**	323	0.35	**1.06**	2.45
Loop seal, u_g=1.7 m/s	69	130	238	0.15	0.50	1.48
Loop seal, u_g=2.7 m/s	78	158	299	0.19	0.72	2.16
Loop seal, u_g=3.6 m/s	81	163	301	0.20	0.77	2.20
Bold values are used throughout this work as the average particle size and terminal velocity						

5.1.1 Bottom bed

At a given riser pressure drop, the height of the dense bed decreases, and is eventually depleted as the fluidization velocity is increased. Simultaneously, the solids concentration in the bed decreases until the bubble voidage reaches $\delta_b = 0.5$ at the point of depletion.

5.1.2 Splash zone

A "splash zone" with an exponential decay, a, is formed in the presence or absence of a dense bed. The model proposed here (the cap-point of the vertical bars) provides better agreement than does the correlation in the literature (dashed line).

Solids entrainment increases in the presence of a dense bed (solid symbols). However, it levels off upon depletion of the bed (empty symbols). A dimensionless correlation is provided.

5.1.3 Transport zone

The clustering back-mixing effect is negligible, as the back-mixing rate decreases in larger units. The core-to-layer transport governs the back-mixing. A Sherwood number-based correlation for this mass transfer coefficient is proposed, showing a good fit to the large-scale data.

5.1.4 Exit Region

The external solids circulation can be approximated to the solids up-flow at the riser top but only for low gas velocities. The backflow ratio at the riser exit increases with the particle velocity (thus, with the gas velocity).
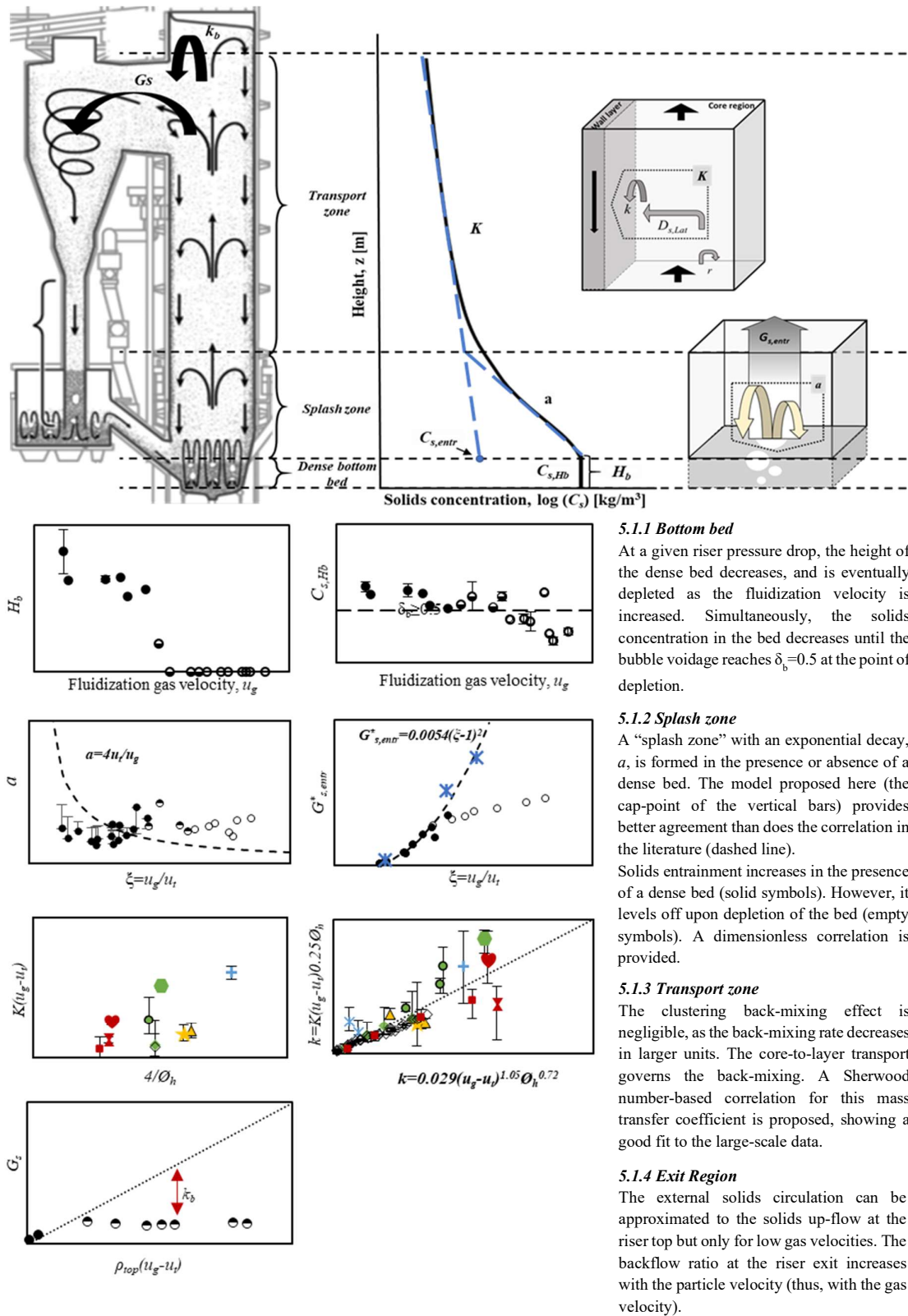
Figure 12. Schematic summary of the main findings of this work. The circular black symbols correspond to fluid-dynamically down-scaled experiments (data compiled from Papers III and IV), and the colored symbols correspond to large-scale CFB boilers (data compiled from Paper V).

5.1.1 Bottom bed

The presence of a dense bed was demonstrated in the 12-MW$_{th}$ Chalmers boiler [36], wherein the dense bed height was shown to decrease with increasing fluidization velocity [36, 37, 71] for a given riser pressure drop. The experimental studies in **Papers I–III** add to this knowledge, revealing that the dense bed is eventually depleted if the fluidization velocity is increased sufficiently, as more material is lifted to higher locations in the riser [71]. This phenomenon has scarcely been studied in the literature on large-scale CFB boilers [36], since monitoring the presence of a dense bed requires the use of densely spaced pressure taps in the bottom region, which is not the case in commercial CFB boilers. As mentioned previously, commercial units typically monitor the pressure drop over a specific height interval (extending over some few meters) in the lower region of the furnace; however, this cannot discern the presence of a dense bed (as at least three pressure measurements are needed to confirm a linear pressure drop). Thus, proper detection of a dense bed requires densely spaced pressure taps in the lower part of the furnace (within the first 1 meter or so). In addition, such a bed will only be present if there is a sufficient amount of bed material in the furnace [44], and it is likely that some commercial CFB boilers operate without a dense bed (for further analysis of this aspect, see Section 5.2).

Figure 13a shows how the dense bed height decreases until bed depletion as the fluidization velocity is increased in the scale model (**Paper III**), which resembles a large-scale CFB boiler (this has also been observed in the pseudo-2D unit – see **Paper I**). The decrease in dense bed height occurs in parallel with a decrease in the solids concentration as the fluidization velocity is increased. Eventually, depletion of the dense bed occurs at solids concentrations that correspond to a situation in which the volume occupied by bubbles equals that occupied by the emulsion phase (dashed line in Figure 13b, corresponding to $\varepsilon_g = 0.715$). This is in line with the observations of Johnsson et al. (1995) [34] in the 12-MW$_{th}$ CFB unit and the pseudo-2D unit.

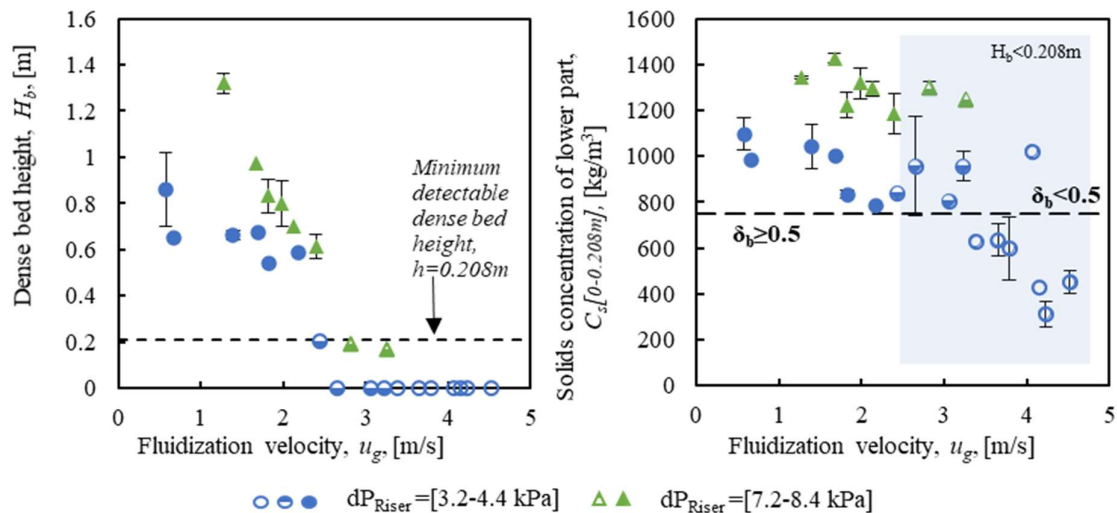Figure 13. Properties of the bottom bed in the cold-scale model as a function of fluidization velocity (up-scaled values): a) dense bed height; b) solids concentration for *h*=0–0.20 m. No dense bed is detected for those cases in which the emulsion phase occupies a smaller volume than the bubble phase. Grey area corresponds to no linear pressure drop below the minimum detectable dense bed height. Compiled from Paper III.

In the presence of a dense bed, bubbles form, rise along the bed, and erupt at the bed surface, ejecting particles into the splash zone according to the erupting bubble size. **Paper IV** evaluates the dependence of bubble size (described through the magnitude of the pressure fluctuations) on dense bed height, both in the Chalmers boiler and the pseudo-2D unit (see Figure 14). The data obtained from the boiler show saturation of the erupting bubble size with bed height for typical bed heights (H_b=0.4–0.6 m), suggesting that the bubble size reaches an equilibrium. Data from the pseudo-2D unit indicate a clear increase in the erupting bubble size for typical bed heights, and suggest that a terminal size of the bubbles may be reached at much greater dense bed heights (above 0.8 m).
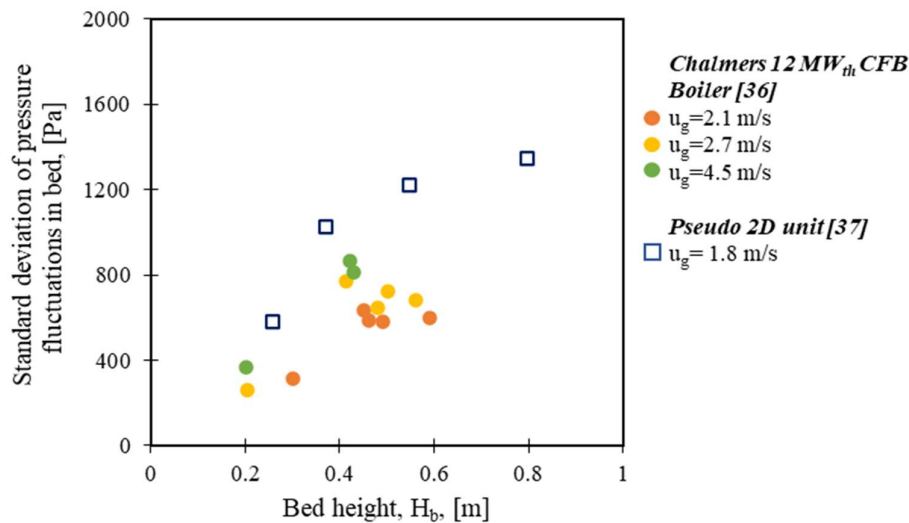

Figure 14. Standard deviations of the pressure fluctuations in the dense bed (indicating the erupting bubble size) as a function of dense bed height. Data measured in the Chalmers boiler [36] and the pseudo-2D unit [37]. Source: Paper IV.

5.1.2 Splash zone

The presence of a splash zone has traditionally been explained in terms of the ejection of particle clusters through bubbles bursting at the dense bed surface and their back-mixing to the dense bed in a gravity-driven ballistic fashion. However, in the absence of a dense bed, a "splash zone" with similar characteristics to that originating from a dense bed has been confirmed. Figure 15 (from **Paper IV**) exemplifies this general phenomenon through three cases conducted in the pseudo-2D unit at different fluidization velocities, one with a dense bed and two without a dense bed. In the absence of a dense bed, the solids concentration profile exhibits a steep decay close to the air distribution, indicating strong solids back-mixing. For these cases, it can be speculated that the ejection of clustered solids arises from the primary gas distributor (the injection holes or nozzles), where a gas flow that is still strongly fluctuating and heterogeneously distributed produces an effect similar to that of erupting bubbles in the presence of a bottom bed, i.e., intermittent and locally high gas velocities that are able to eject strands of solids. In the presence of a dense bed, the splash zone is assumed to originate from solids ejection by erupting bubbles, implying that the erupting bubble size (and velocity, which increases with size [39]) is a key parameter for describing the solids back-mixing immediately above the dense bed.
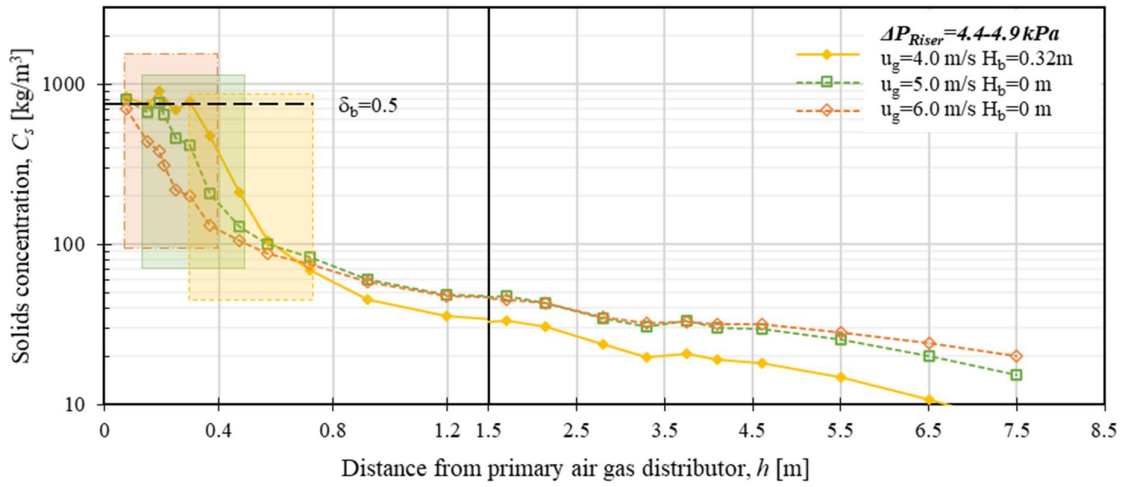
Figure 15. Vertical profiles of solids concentration in the pseudo-2D unit. Note the scale shift on the abscissa. Shown are three cases with different fluidization velocities and a constant riser pressure drop, one of which generates a dense bed and two that do not. Source: Paper IV.

Figure 16 shows that an increasing dense bed height yields a splash zone with a lower level of solids back-mixing in the pseudo-2D unit (star symbols with dashed lines) than in the fluid-dynamically down-scaled tests (symbols not connected with a line) from the scale model, for which the decay coefficient remains unaffected by the dense bed height. This can be explained by the finding shown in Figure 14 that the erupting bubble size remains independent of the dense bed height for the cold-scaled model, while it continues to increase in the pseudo-2D unit for the investigated range of bed heights.
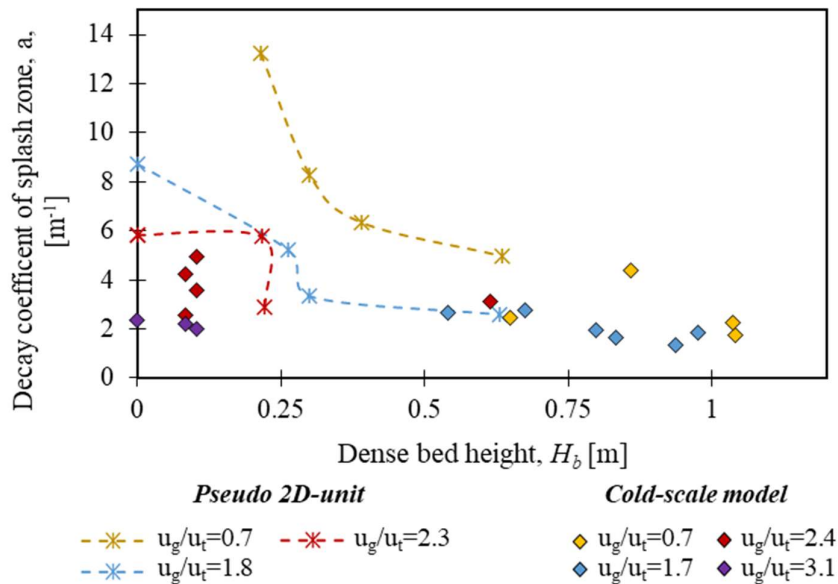

Figure 16. Decay coefficient of the splash zone, a, as a function of the dense bed height for different relative gas velocities, u_g/u_t. Data compiled from Paper IV.

Experimental values of the decay coefficient in the splash zone from the fluid dynamic down-scaled model are shown in Figure 17 (collated data from **Papers III** and **IV**). The dependence on fluidization velocity observed earlier in the Chalmers boiler and included in the empirical correlation provided previously [17, 39] (dashed line) is not clearly evident from the measurements in the scale model. These measurements further show that different dense bed heights (i.e., riser pressure drops) yield similar decay coefficients, as discussed above. The splash-zone decay coefficient for the cases that contain a dense bed is modeled through Monte Carlo simulations with the assumption of ballistic trajectories of the solids clusters, where expressions from the literature are used for the solids ejection angle and velocity (see **Paper IV**). The simulations yield vertical concentration profiles that can be approximated to exponential decays with decay coefficients that show better agreement with all the measurements than those provided by the empirical expression, Eq. (16), from the literature [17] (average error values of 46% and 73%, respectively).

The modeled value of the decay coefficient for each case with a dense bed is indicated in Figure 17 as a black vertical bar. The fact that modeling is able to provide a good description despite neglecting the drag force exerted by the surrounding gas is explained by the decreased significance of the (surface-related) drag term in front of the (volume-related) gravitational term for large structures such as the clusters, as here studied. Finally, it is noteworthy that an average value of a=2.2 m^{-1} (red dashed-dot line in Figure 17) results in an average estimation error of 26% for all the cases with a dense bed.

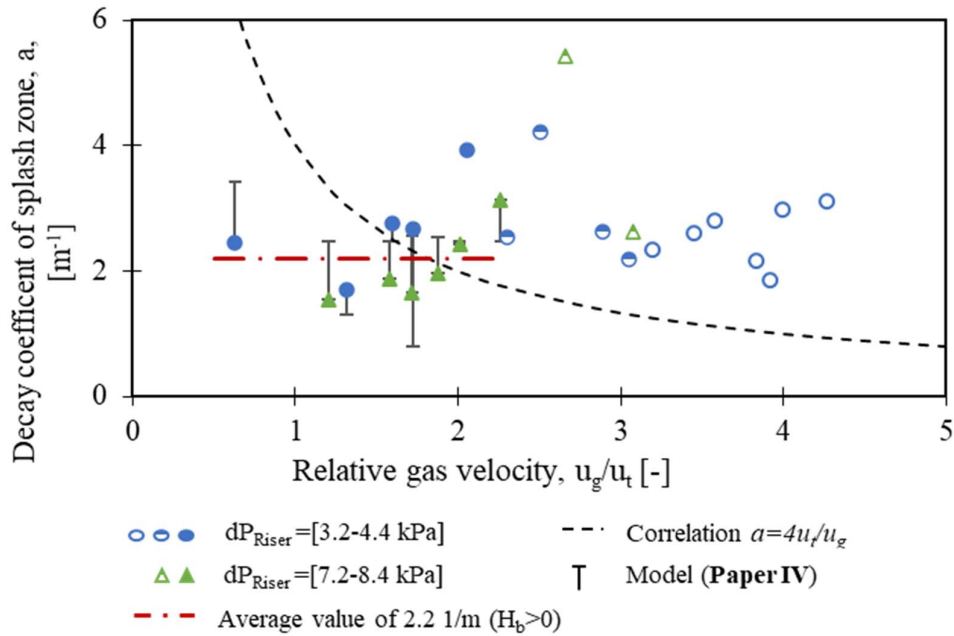Figure 17. Decay coefficient in the splash zone as a function of the relative gas velocity, u_g/u_t. Values shown are from experiments in the cold-scale model (colored symbols), modeled (cap of the black error bar, only for cases with a dense bed), and correlated [Eq.16, [17]] (black dashed line). The red dashed-dot line indicates the average for the experimental values. Data compiled from results in Paper IV.

The experimental data in **Papers I**–**III** show that the solids entrainment increases with fluidization velocity as long as a dense bed is maintained (with the height of the dense bed not affecting the rate of entrainment) and levels out when the dense bed is depleted. This is exemplified by the experimental data from the cold-scale model shown in Figure 18 (**Paper III**)**,** where the different entrainment levels rely on the riser pressure drop when the dense bed is lost.
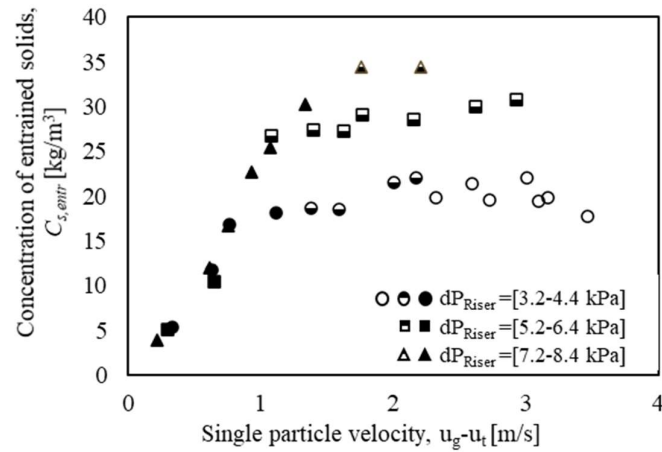

Figure 18. Solids entrainment from the bottom region as a function of the single particle velocity. Measurement data from the scaled tests, without any secondary air injections. Source: Paper III.

Other factors that could affect the entrainment are the lateral injection of air (recirculated flue gas, air staging) and the tapered wall configuration. Figure 19 shows the reference data series (vertical walls without lateral gas injections), as indicated with black square symbols. The effect of using a tapered wall configuration (red symbols in Figure 19a) on the entrainment of solids is studied, and it is concluded that a given volume flow of primary gas yields the same solids entrainment regardless of the bottom configuration employed. In Figure 19b, gas injections from the sidewalls are applied below or above the dense bed surface (triangle and diamond symbols for two different injection heights), showing that the solids entrainment is increased only if the gas is injected into the dense bed and decreases otherwise, with the effect being magnified according to the magnitude of the gas injection.
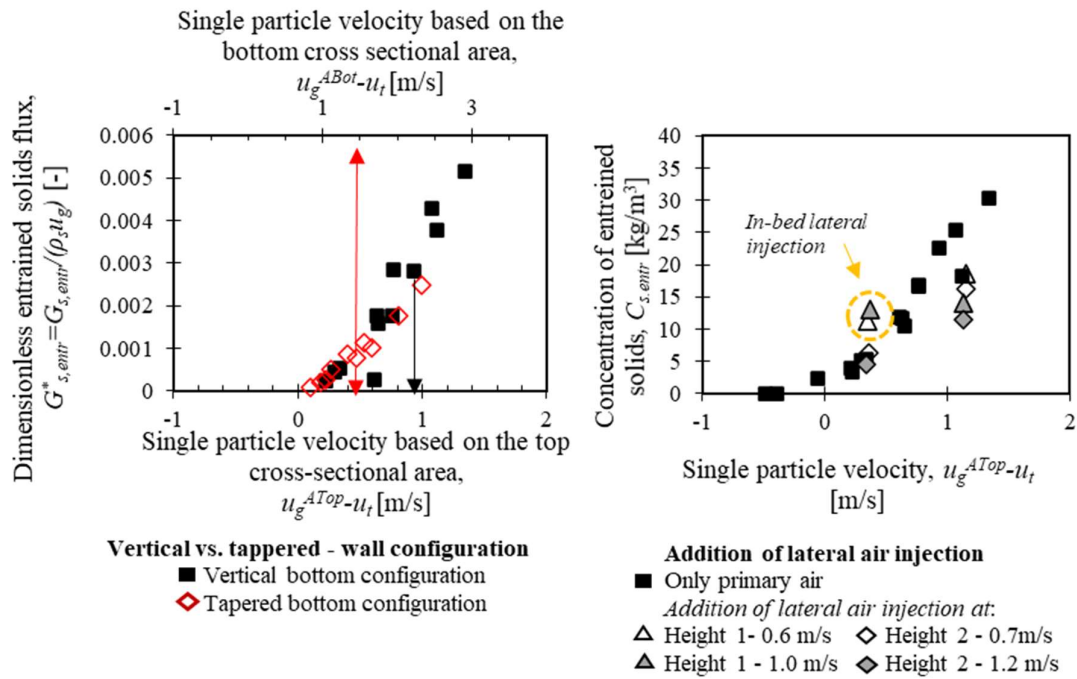
Figure 19. Solids entrainment versus single particle velocity for: a) comparison of the tapered and vertical bottom configurations (Source: Paper IV); b) lateral injection of air at two different heights –the yellow circle shows the cases with lateral injection into the dense bed, with the remainder injected above the dense bed. Source: Paper III.

Considering the levelling-out of the solids entrainment as the dense bed becomes depleted and the complex influence of the lateral gas injections, the following empirical correlation based on the non-dimensionalization of the solids flux (see Glicksman [55]) is derived from the cases with only primary air and the confirmed presence of a dense bed (i.e., in the Chalmers 12-MW$_{th}$ CFB boiler and the cold-scale model) (see Figure 20a):

$$G_{s.entr}^* = \frac{C_{s,entr}(u_g - u_t)}{\rho_s u_g} = 0.0054 \left(\frac{u_g}{u_t} - 1\right)^2 \qquad (23)$$

In Figure 20a, the data for the scaled cases without a dense bottom bed are included to allow comparison of the values when the dense bed is depleted. Figure 19b shows the level of agreement of this correlation with the data from large-scale CFB boilers reported in the literature, i.e., including lateral injections of gas and tapered bottom configurations, and with uncertainty regarding the presence of a dense bottom bed. There is also an inherent uncertainty related to the determination of the solids entrainment from the literature data (expressed in the form of vertical bars in the figure), due to the few data-points typically available in the measured vertical profiles. Nevertheless, the correlation proposed in Eq. (23) shows satisfactory agreement with the values from the large-scale CFB boilers gathered from the literature.
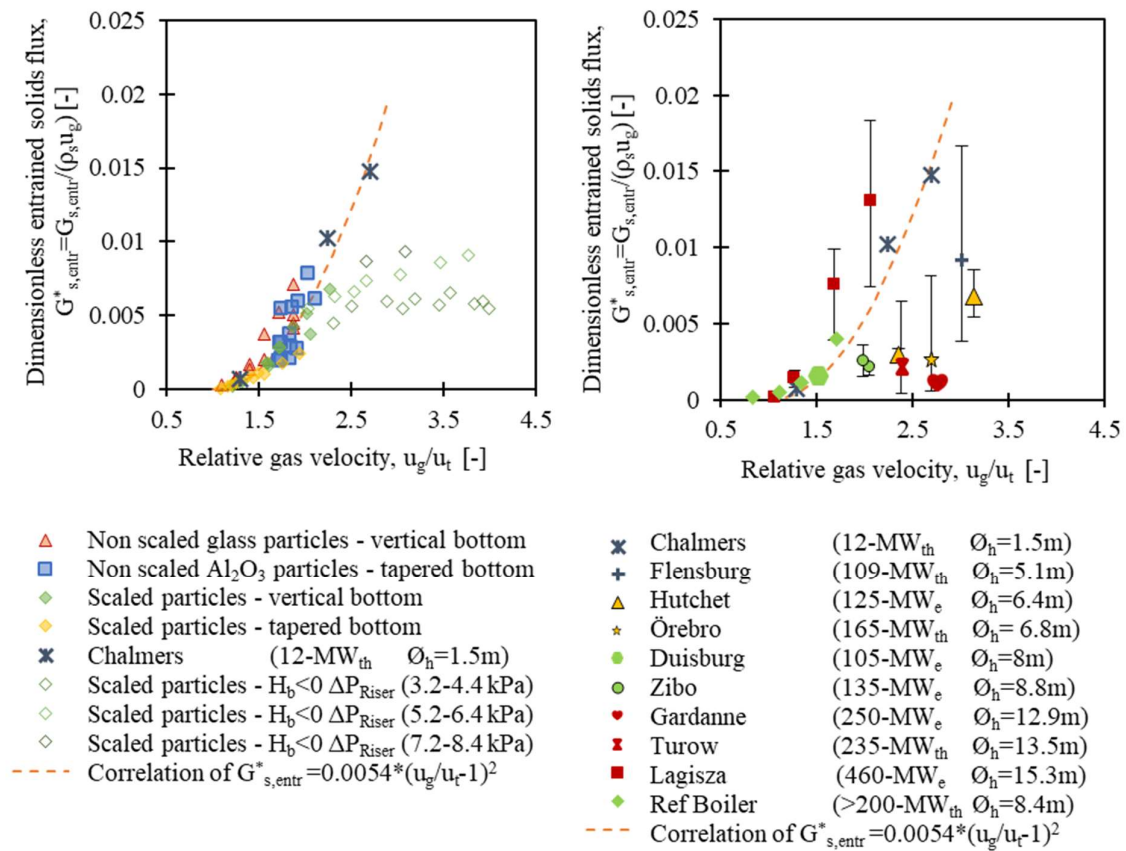

Figure 20. Dimensionless solids entrainment from the bottom region: a) values used for the correlation derived in Paper IV (except for cases without a dense bed - empty symbols (Source: Paper III) - which are added for comparison only); b) correlation compared to values calculated from the profiles given in the literature for large-scale CFB boilers (see Table 5).

5.1.3 Transport zone

Experimental studies conducted in the pseudo-2D unit (**Paper I**) and through non-scaled and scaled tests in the cold-scale model (**Papers II** and **III**, respectively) show that the solids back-mixing (assessed through the decay coefficient, K) in the transport zone is not affected by either the riser pressure drop or the presence or absence of a dense bed, although it shows a slight decrease with fluidization velocity. **Paper V** focuses on the transport zone and analyzes the experimental concentration profiles in commercial CFB boilers published in the literature (including this work, i.e., **Paper III**). Figure 21 compares these decay coefficients from the commercial CFB boilers and the scaled experiments studied in **Paper V** to the values obtained from the non-scaled 3D unit test (**Paper II**) and the pseudo-2D unit (**Paper I**). The latter and the Chalmers 12-MW unit (i.e., the smallest of the units considered) show much higher solids back-mixing, revealing the influence of furnace size.
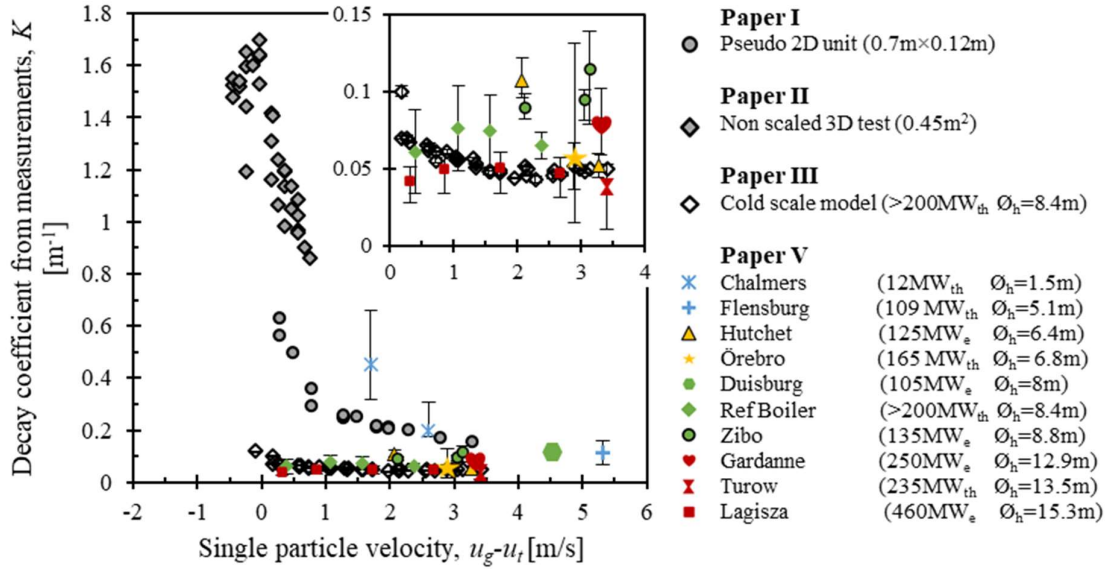
Figure 21. Decay coefficients in the transport zones of the CFB furnaces considered in this work. Data compiled from Papers I–III,V.

Two possible solids back-mixing pathways are considered in the transport zone (see

Figure 12): (i) through clustering in the core region (occurring at a volumetric rate, r); or (ii) through transfer from the core to the wall layer, which entails lateral dispersion in the core region to the vicinity of the wall layer (according to a dispersion coefficient, $D_{s,lat}$), followed by boundary transfer to the wall layer (characterized by a mass transfer coefficient, k). In **Paper V**, the decay coefficient that emerges from these back-mixing paths is derived as:

$$K\left(u_g - u_t\right) = \left(\frac{1}{k} + \frac{\varnothing_h/2}{2\,D_{s,lat}}\right)^{-1} \frac{4}{\varnothing_h} + r \tag{24}$$

The relative extents of these two back-mixing paths have been discussed in the literature [40] but have not been assessed previously. Figure 22 illustrates the relative importance of each back-mixing pathway, through experimental data from commercial CFB boilers plotted according to Eq. (24). The data-points show a tendency to the origo of the figure and, thus, indicate that the solids clustering (*r*-value) makes a small contribution to the solids back-mixing.

Figure 22. The solids back-mixing rate according to Eq. (24): back-mixing rate, $K(u_g-u_t)$, as a function of the perimeter-to-area (inverse unit size). Source: Paper V.

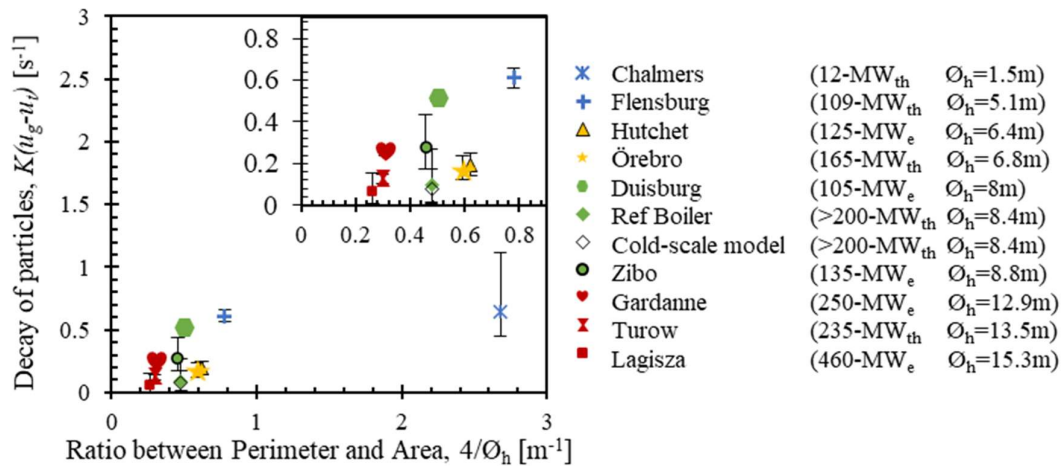Furthermore, **Paper V** studies the role of the two mechanisms constituting the core-to-wall layer back-mixing, which is shown to be dominant. For this purpose, this work uses semi-empirical modeling of the closure of the solids mass balance in the core region, while neglecting the mass transfer through the core-wall layer boundary. The results show the *Pe*-numbers used earlier in the literature to model the Chalmers boiler (*Pe*=150) [72] provide a too-slow dispersion rate to describe the decay coefficient in larger units, even if the mass transfer through the core-wall layer boundary is neglected, as displayed in Figure 23a. Instead, the turbulence-based equations proposed by Palchonok et al. [73] provide a valid description of the lateral solids dispersion for all the cases studied (Figure 23b). These lateral solids dispersion rates are sufficiently high to resemble the flat horizontal profiles of the solids concentration observed experimentally in commercial-scale boilers. A flat horizontal profile of the solids flux is a typical feature of commercial-scale CFB boilers. It indicates that the lateral solids dispersion is faster than the core-to-wall layer transfer coefficient (otherwise, a parabolic flux profile would have emerged). Thus, the governing (limiting) process for the back-mixing in the transport zone is the mass transfer into the wall layer from its vicinity, which is further explored in **Paper V**.
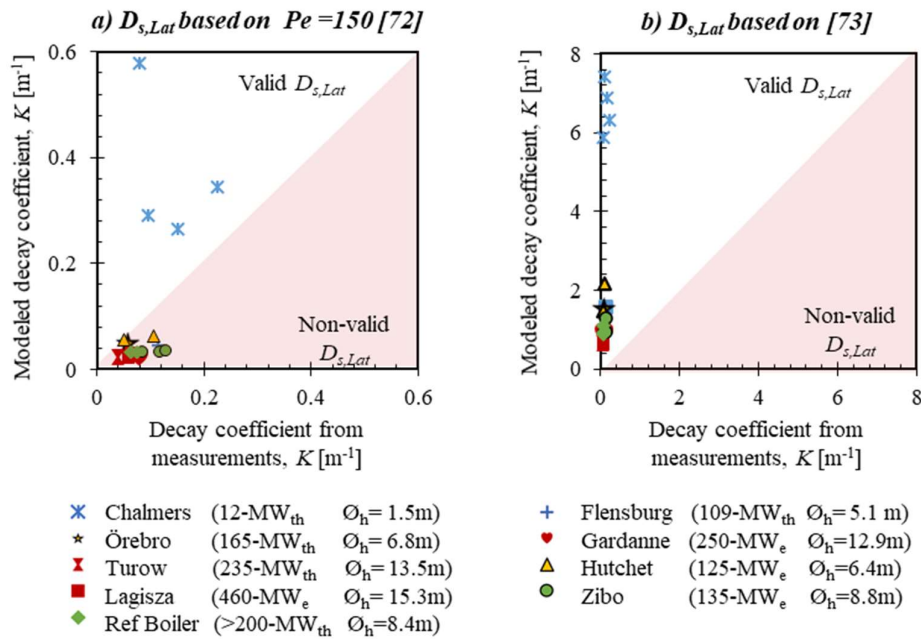
Figure 23. Decay coefficients modeled with infinite core-to-wall layer mass transfer, as compared to the measured values. Lateral solids dispersion estimated through: a) *Pe*=150 [72]; b) based on [73] within Paper V. Source: Paper V.

Solids mixing through turbophoresis, which drives particle migration in the direction of decreasing turbulence level [68-70], was found to be a valid explanation for the transfer of solids from the dilute core region to the denser wall layer, i.e., opposite to the direction expected from classical dispersion from high- to low-concentration fields. The governing parameter for turbophoresis is the spatial derivative of the variance of the solids velocity fluctuations in the given direction. **Paper V** uses DNS models to study this derivative at the core-wall layer boundary, with the results given in Figure 24, from which it can be observed that the solid velocity fluctuations normal to the wall remain approximately constant with simulation time. That the turbophoretic core-to-wall layer transport is independent of the wall layer properties (thickness, concentration, velocity) is in line with the constant decay coefficient with height observed in large-scale CFB furnaces, and represents a validation of turbophoresis as the underlying mechanism for the core-to-wall layer net transfer of solids.
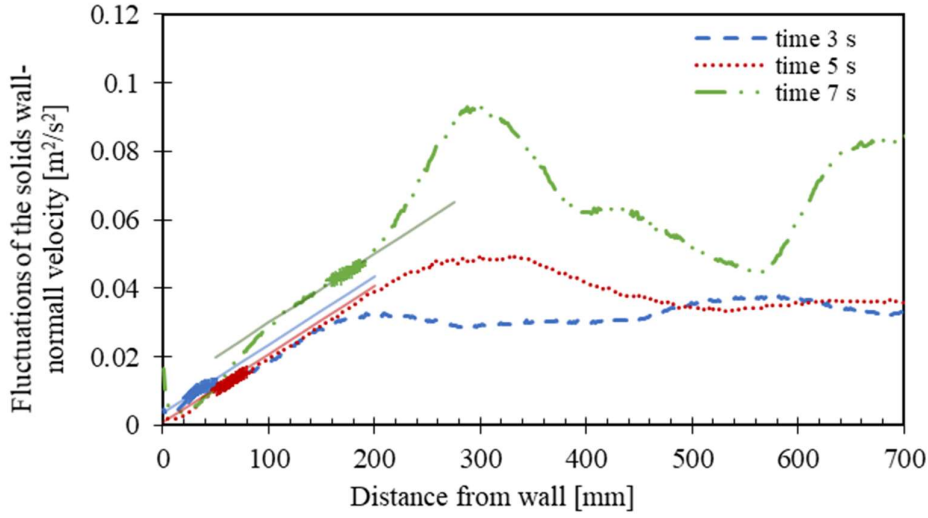
Figure 24. DNS-modeled variance of the fluctuations in lateral solids velocity
for different simulation times. Source: Paper V.

Furthermore, **Paper V** identifies the similarity between semi-empirical expressions for the turbophoretic deposition rate and the Linton-Sherwood *Sh*-number expression for internal turbulent flow. In addition, **Paper V** shows (Figure 25) how these factors, combined with the expressions from Palchonok et al. [73] for the solids lateral dispersion, are able to describe the core-to-wall layer mass transfer coefficients measured in large-scale CFB boilers through:

$$k = 0.029 * \left(u_g - u_t\right)^{1.05} * \varnothing_h^{0.72} \tag{25}$$

Neglecting the clustering effect and assuming a fast solids dispersion in the core region, the decay coefficient for the solids concentration is expressed as:

$$K = \frac{k\frac{4}{\varnothing_h}}{u_g - u_t} \tag{26}$$
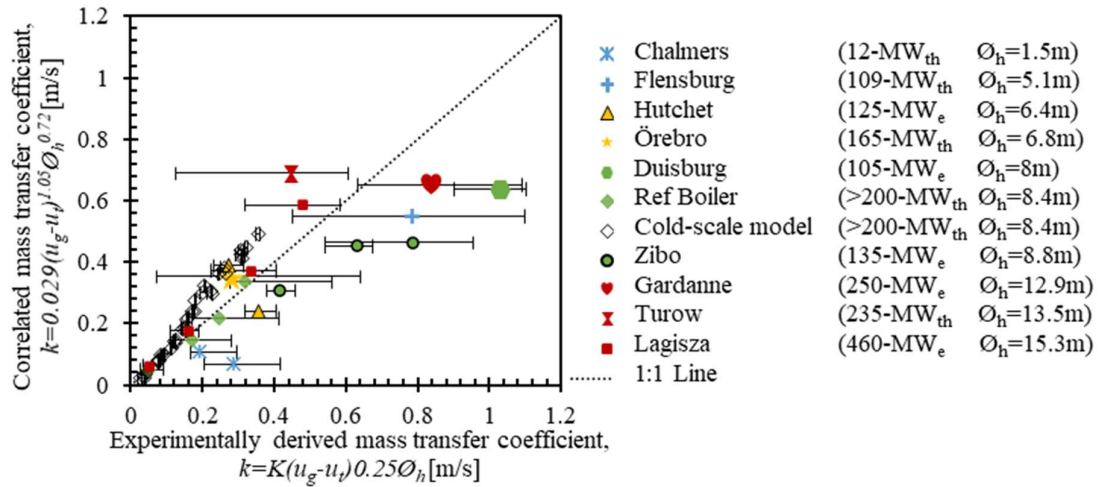
Figure 25. Experimentally derived [Eq. (26)] and correlated [Eq. (25)]
values of the core-to-wall layer mass transfer coefficient, *k*. Data compiled from Paper V.

Thus, combining Eqs. (25) and (26) yields:

$$K = 0.116 * \emptyset_h{}^{-0.28}(u_g - u_t)^{0.05} \tag{27}$$

The agreement between the decay coefficients derived from experimental data and the different correlations proposed in the literature, including Eq. (27), is depicted in Figure 26. The expression derived in this work yields an average error of 28%, as compared with 280% for Eq. (17) [17], 86% based on the work of Davidson [33], and 57% for Eq. (18) [40].

$K_1 = 0.116 * \emptyset_h{}^{-0.28}(u_g - u_t)^{0.05}$ - this work

$K_2 = \dfrac{0.23}{(u_g - u_t)}$ - Johnsson & Leckner (1995) [17]

$K_3 = \dfrac{1}{H_t}$ - Johansson et al (2005) [40]

$K_4 = 0.01\sqrt{\pi}\dfrac{4}{\emptyset_h}$ - Davidson (2000) [33]
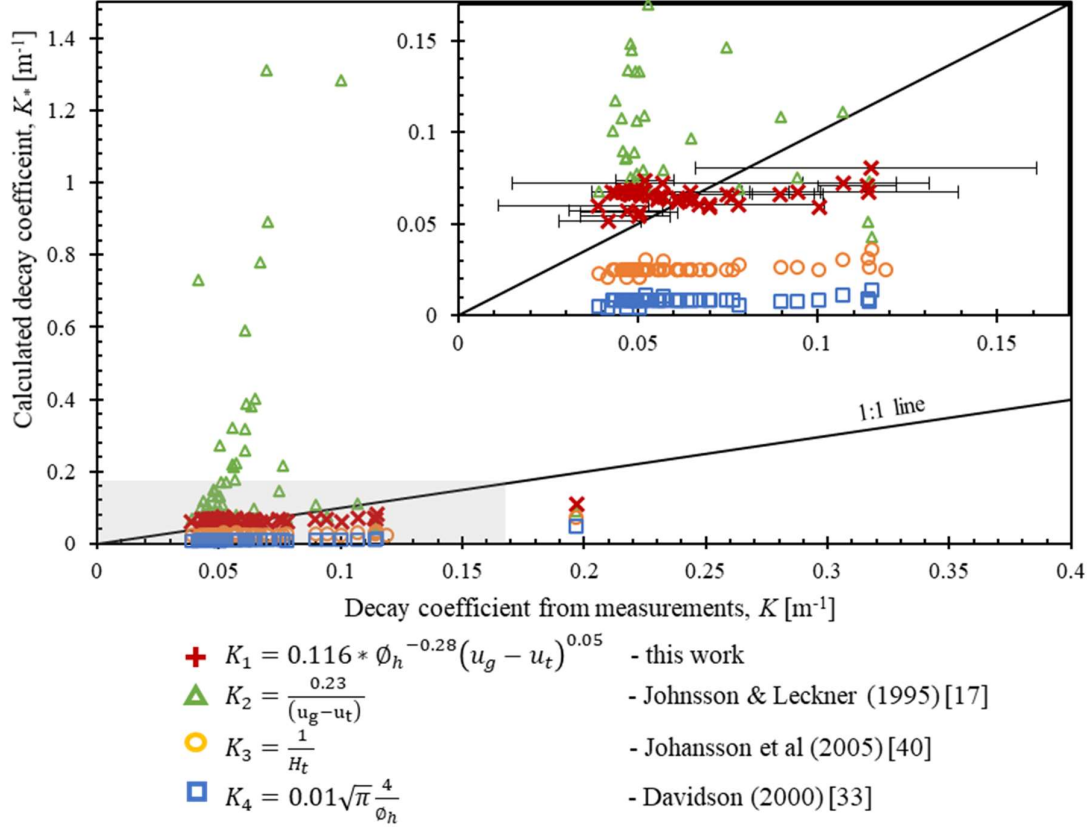
Figure 26: Correlated and experimental values of the decay coefficient in the transport zone. The gray area is magnified in the upper-right corner. Source: Paper V.

5.1.4   Exit region

The solids backflow in the exit region was experimentally evaluated in **Papers I–III.** In general, the solids up-flux at the top of the riser increases with fluidization velocity, as exemplified in Figure 27 using data collected from the cold-scale model. The figure also shows the flow of solids that are circulating externally, measured according to the method summarized in Section 3.2. At higher gas velocities, a remarkable difference is evident between the solids flow that reaches the top of the riser and the external solids circulation, indicating significant solids back-flow.

At low gas velocities (i.e., low values of the solids upwards flux), all the solids that reach the riser top are externally circulated, which means that the backflow is negligible. No influence of the bottom region fluid dynamics is observed. This strong solids back-flow at high gas velocities raises questions as to the validity of an approximation that appears commonly in the literature, estimating the solids external circulation from the solids concentration in the upper part of the riser (as derived from pressure measurements) with the single particle velocity u_g-u_t, i.e., disregarding the back-flow effect. Moreover, in the cited approximation, u_t is often based on an average-sized bed particle. Thus, there is also an error due to not considering the particle segregation effect (*cf*. Table 6). The size segregation effect between the bottom region and the top region becomes larger the lower the gas velocity and, thus, the larger will be the over-estimation of the terminal velocity (yielding an under-estimation of the external solids flux). This under-estimation compensates to some extent (and even potentially surpasses) for the over-estimation linked to the disregarding of the back-flow effect in the estimation. In summary, the literature data on the external circulation on solids in large-scale CFB boilers estimated from pressure measurements at the furnace top should be treated with caution, as both the back-mixing effects and particle segregation effects may be substantial.
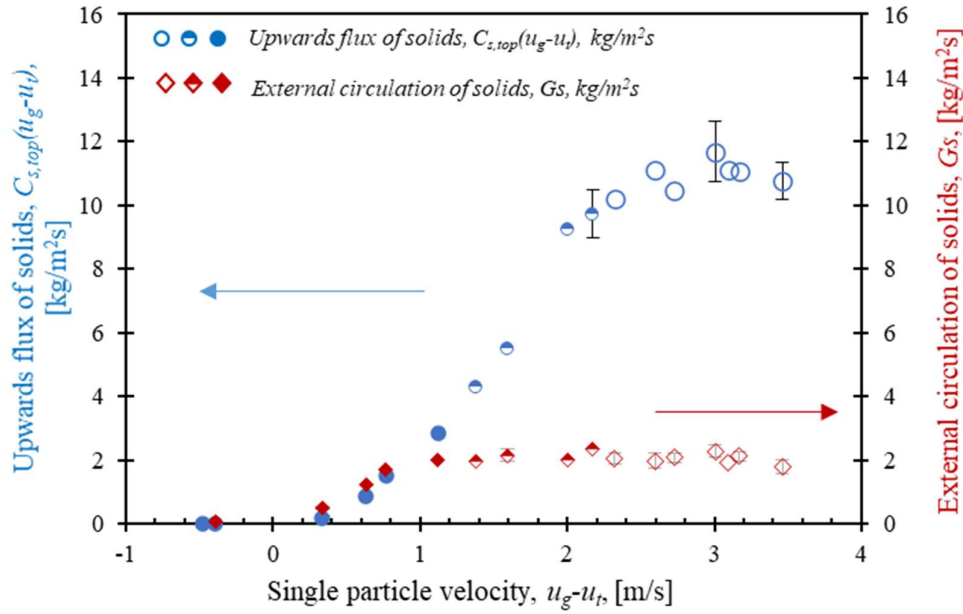
Figure 27: Upwards flux of solids at the riser top (estimated from the local solids concentration) compared to the external solids flux (measured through fluidization of the cyclone leg, see Section 3.2). Results are from the cold-scale model with up-scaled riser pressure drop of 3.2–4.4 kPa. Data compiled from results in Paper III.

The back-flow phenomenon arises from the inability of the gas to drag the solids along, as it curves into the exit duct to the cyclone. Therefore, the Stokes number, *St*, is chosen to describe the relationship between the inertia of the particles and the drag exerted by the gas:

$$St = \frac{\rho_s d_p^2}{18\mu_g}\frac{u}{l} \tag{28}$$

47

Since the particle Reynolds number, Re_p, is greater than unity, that is the drag is not purely in the Stokes regime, an effective Stokes number, St_e, [74] accounting for the hybrid (viscous and inertial) drag needs to be considered instead of the classic St-number:

$$St_e = \psi St, \tag{29}$$

The correction factor used is based on the Reynolds particle number and drag coefficient [74]:

$$\psi(Re_p) = \frac{24}{Re_p^0} \int_0^{Re_p^0} \frac{dRe'}{C_D(Re')Re'} \tag{30}$$

where the drag coefficient has been taken as $C_D = 24/Re_p(1+0.158Re_p^{2/3})$ [75] and the correction factor developed as:

$$\psi(Re_p) = \frac{3\sqrt{0.158}Re_p^{1/3} - tan^{-1}\left(\sqrt{0.158}Re_p^{1/3}\right)}{0.158^{2/3}Re_p} \tag{31}$$

As for the characteristic length in Eq. (28), the distance between the riser exit walls and the middle of the riser is taken as $l=W/2$.

Figure 28 plots the back-flow ratio in relation to the effective Stokes number. As seen, the back-flow is almost non-existent at low St_e-numbers, and there is a transition in the range of 0.07–0.11, such that the back-flow increases rapidly before eventually levelling out at St_e-numbers greater than about 0.12. It should be noted that the back-flow effect observed, i.e., the separation in the riser of the solids from the gas flow, is unit-specific and depends on the geometry of the exit configuration, including the riser exit duct, as described previously [32].
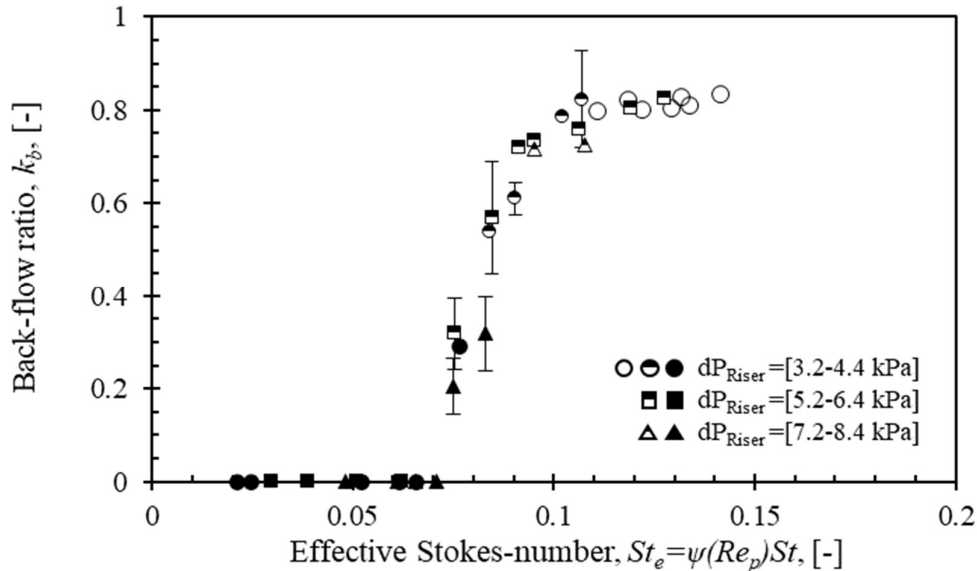

Figure 28 Solids back-flow ratio as a function of the Effective Stokes number, Eq. (29). Data from the scaled tests representing a >200-MW$_{th}$ CFB boiler. Data compiled from Paper III.

48

5.2 Closure of the solids mass balance in the furnace

The solids flow in the CFB furnace can be studied through the vertical profile of the solids concentration, according to Eq. (9) in Section 2.1. This subsection presents and discusses the possibility of predicting the vertical profiles of the solids concentrations in large-scale CFB furnaces without the need for site data, i.e., based solely on the above results and expressions. This is performed using three utility-scale cases from the literature: the CFB furnaces in Huchet [21], Turow [23] and Zibo [25], all of which are detailed in Table 7. These exemplary cases have been chosen based on the spatial resolution of the experimental profile, with the Huchet and Turow units providing the most data-points. The Zibo CFB boiler has been included to enable the discussion as to how the lack of spatial resolution in the measurements at the bottom region influences the data analysis. It should be noted that the three examples chosen for the discussion have contributed to the fitting of the *Sh*-number expression for the decay coefficient in the transport zone [see Eq. (25), Figure 25] , albeit only to a limited extent, given the many more cases considered from, for example, the Chalmers boiler and the scaled tests. Furthermore, the three example cases chosen have not been considered in either the derivation of the expressions for the solids entrainment [see Eq. (23), Figure 20] or in the correlation of the decay coefficient in the splash zone (in the work of Johnsson and Leckner [17]).

The upper section of Table 7 lists the input parameters (*cf.* Figure 4) for the three cases considered (furnace geometry, solids properties, gas flow and riser pressure drop). The first challenge is how to estimate the total riser pressure drop, since the measured riser pressure drop is typically not measured from the nozzle height level (one exception to this is the Turow unit) and, therefore, a significant pressure drop in the dense bottom region is not accounted for in the measured value. As a consequence, the total riser pressure drop is estimated through extrapolation of the solids concentration profile towards the nozzle height level. This is done by extrapolating the profile according to Eq. (8), down to the height for which the value corresponding to the estimated solids concentration in the dense bed [38] is reached (thereby indicating the location of the dense bed surface) or down to the nozzle height level (which is indicative of the absence of a dense bed). By integrating the complete solids concentration profile, the estimated values for the total riser pressure drop given in Table 7 can be obtained.

Figure 29a depicts the measured vertical profiles of the pressure drops for these cases. The corresponding values for the solids concentrations derived from the pressure measurements are plotted with symbols in Figure 29b. The fitting of these data-points to Eq. (9) results in the values for the fitting parameters (*a*, $C_{s,entr}$, *K*) listed in Table 7 (*Experimental* columns) and the solid lines in Figure 28b. Furthermore, the dashed lines represent the solids concentration profiles predicted according to Eqs. (16) and (27) (decay coefficients *a* and *K,* respectively*)*, Eq. (23) (the solids entrainment $C_{s,entr}$), and the expressions in [38] (the solids concentration in the dense bed), yielding the parameter values listed under the *Model* columns in Table 7. Based on these values, the dense bed height can be calculated through the riser pressure drop using Eq. (14)
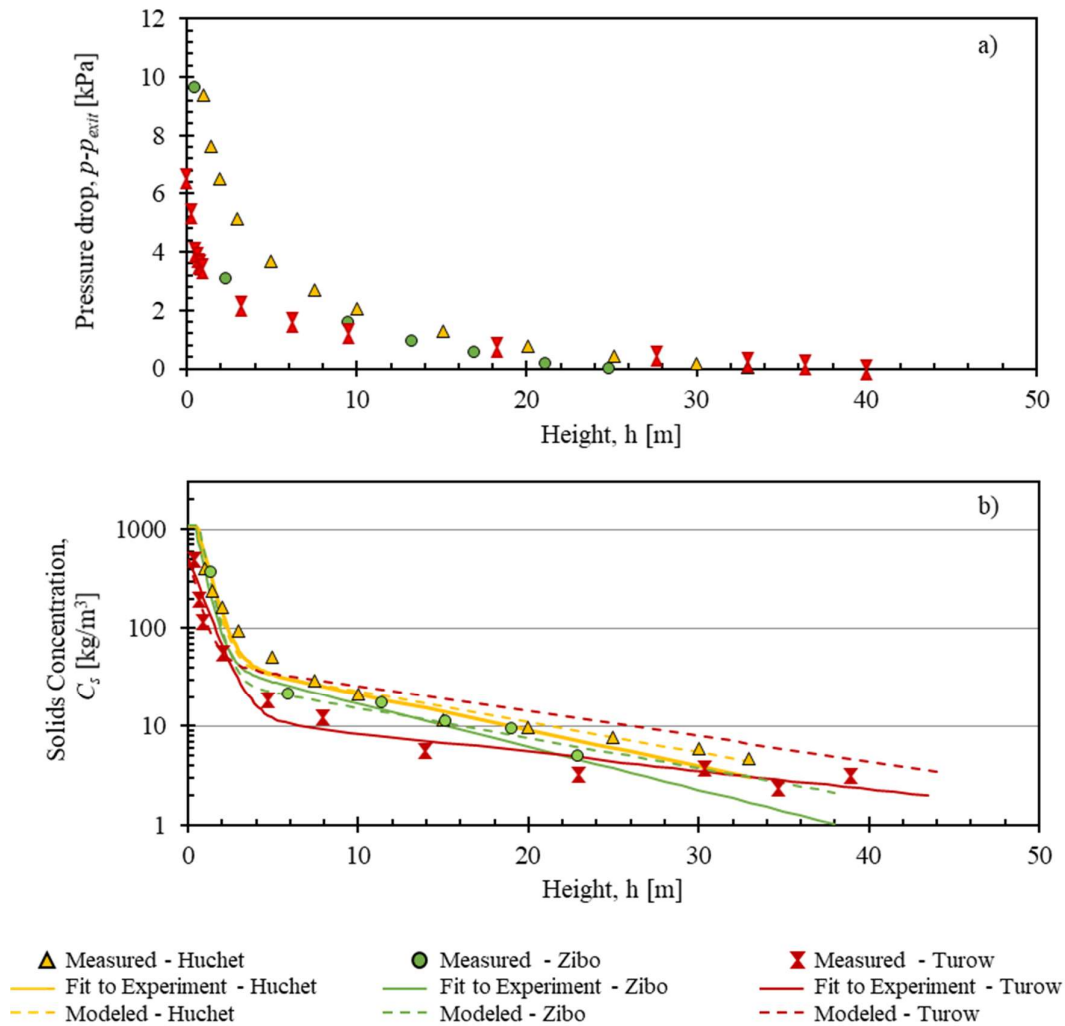
Figure 29. Vertical profiles for the three cases studied (Huchet [21], Zibo [25] and Turow [23]) for: a) the measured pressure drop; and b) the solids concentration: experimental (derived from data in (a), markers), fits of Eq. (9) to the experimental data (solid line) and modeled data (dashed line).

Note the low spatial resolution of the solids concentration profile for the Zibo furnace, especially in the bottom region (one concentration value in the height range of 0–5.8 m), which implies a high level of uncertainty regarding the fitting of the decay coefficient for the splash zone to the experimental data. Fitting against the two values in the pressure profile (which by definition must have the same decay constant, given the exponential decay) gives a value of 1.9 for the decay coefficient in the splash zone. It should be noted that a variation of ±20% in this value results in a variability of 20%-35% in the calculated dense bed height.

While the analyses indicate that the Huchet and Zibo cases yield a dense bed (with height of around 0.5 m in both cases; see Table 7), the processing of the measurement data from the Turow case suggests that there is no dense bed present [as defined by Eq. (1)]. This seems reasonable given that the experimental solids concentrations at the lowest heights, measured between ports located at 0 m and 0.37 m, are 500 kg/m^3 (thus, far less than the values typical for dense beds in large-scale boilers), as well as the fact that the furnace has a relatively low pressure drop considering that it has a height of almost 40 m.

Table 7. Parameters used for the analysis and predictions of the solids concentration profiles in the three CFB furnace cases.

Parameter		Huchet		Zibo		Turow	
Unit size	$\varnothing_h$ [m]	6.4		6.6		6.6	
Furnace height	H [m]	33		38		38	
Particle density	ρ_s [kg/m³]	2,600		2,600		2,600	
Particle size	d_p [µm]	250		300		300	
Terminal velocity	u_t [m/s]	1.53		1.89		1.89	
Fluidization velocity	u_g [m/s]	3.6		2.9		2.9	
Measured Riser pressure drop	$\Delta P_{riser,\,exp}$[kPa]	9.3 (h=[1–33] m)		9.6 (h=[0.4–25] m)		6.5 (h=[0–40] m)	
Estimated total Riser pressure drop	$\Delta P_{riser\text{-}Tot}$ [kPa]	17.0		13.4		6.5	
Experimentally-fitted (Exp) and modeled (Mod) values		*Exp*	*Mod*	*Exp*	*Mod*	*Exp*	*Mod*
Decay coefficient splash zone	a [m⁻¹]	**1.6**	1.7	**1.9**	1.9	**1.12**	1.7
Decay coefficient transport zone	K [m⁻¹]	**0.085**	0.071	**0.101**	0.071	**0.043**	0.059
Entrained solids concentration	$C_{s,entr}$ [kg/m³]	**48**	44.7	**45.0**	30.0	**12.5**	46.2
Dimensionless entrained flux	$G^*_{s,entr}$ [-]	**0.011**	0.010	**0.009**	0.006	**0.003**	0.010
Solids concentration in dense bed	$C_{s,Hb}$ [kg/m³]	**1082**	1080	**1084**	1084	**480***	**
Dense bed height	H_b [m]	**0.55**	0.51	**0.4**	0.62	**0**	0

*Experimentally-fitted solids concentration at h=0 m in the absence of a dense bed [using H_b=0 in Eq. (14)].
**The modeled values for the disperse-phase parameters (solids entrainment and decay coefficient in the transport zone) yield a higher pressure drop for this phase than the given experimental value for the total riser pressure drop. Thus, the model cannot describe this case due to the absence of a dense bed.

The predicted solids concentration profiles are in good agreement with the experimental data for the Huchet and Zibo cases, while this is not the case for the Turow unit due to the abovementioned putative absence of a dense bottom bed and the non-validity of the model under this condition. In general, the modeled decay coefficients in the splash and transport zones are in good agreement with the experimental ones. The model over-predicts the dense bed height for the Zibo CFB furnace by 0.22 m (compared to the experimentally-fitted value of 0.4 m). This is attributed to a slight under-prediction of the entrained solids concentration, resulting in the need for a slightly higher dense bed height to attain the measured total riser pressure drop. However, the abovementioned poor resolution of the measurements and the consequent uncertainty related to the values for some of the experimentally-derived parameters should be kept in mind.

Regarding the solids entrainment from the bottom region, the modeled values are satisfactory for the Huchet and Zibo cases but are strongly over-estimated for the Turow case (with a modeled value for $C_{s,entr}$ of 46.2 kg/m³ instead of the experimentally-derived value of 12.5 kg/m³; see Table 7).

This results in an unsatisfactory prediction of the solids concentration profile, and it cannot fulfil the total riser pressure drop provided as an experimental input even in the absence of a dense bed. Bearing in mind the above-discussed indications of a depleted dense bed in the Turow case, this over-estimation of the solids entrainment is in line with one of the findings in this work revealing that the solids entrainment is reduced by the depletion of the dense bed (*cf.* Figure 20). Cases with a depleted dense bed lie outside the scope of the correlation for solids entrainment derived in this work [Eq. (23)], which explains the over-estimation of the solids entrainment in the model.

The modeled overall solids mass balance for the two cases with dense bed (Huchet and Zibo) is show in Figure 30.

	Huchet [kg/s]	Zibo [kg/s]
F_{entr}	5092	5162
F_{top}	500	366
F_{lat}	4592	4795
F_s	100 (Gs=1.8 kg/m²s)	73 (Gs=0.85 kg/m²s)
$F_{backflow}$	400	293
F_{layer}	4992	5088
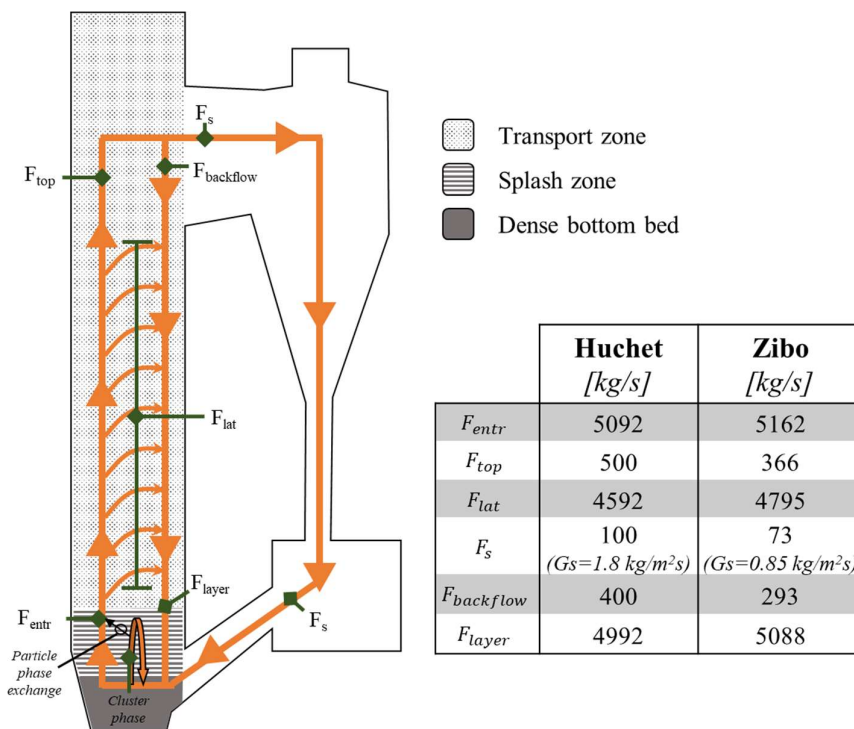
Figure 30. Modeled solids flows in the Huchet and Zibo CFB boilers, based on an assumption of 80% internal back-flow

In summary, the expressions used to describe the vertical profile of the solids concentration [Eq. (9)] and its key parameters (decay coefficients, Eqs. (16) and (27); solids entrainment, Eq. (23); solids concentration in the dense bed, [38]; and dense bed height, Eq. (14)) are shown to be in good agreement with the measurements, provided that a dense bed is present. Thus, the work presented in this thesis enables, through deepened knowledge and expressions with wide validity ranges, the closure of the overall solids mass balance in large-scale CFB furnaces and thus the determination of the main solids flows (see table in Figure 30). More work is however required to understand, and thereby predict, the solids flows in boilers that lack a dense bed of the type defined by Eq. (1). The solids entrainment from the bottom region is identified as a key parameter for further investigation, in order to attain a better understanding and reliable predictions of how the depletion of the dense bed and, to a lesser extent, the lateral injections of gas affect this phenomenon.

CHAPTER 6
Conclusions

This thesis enhances our understanding of the solids flow pattern in the riser of large-scale CFB furnaces for thermochemical conversion of solids by providing general descriptions of the mechanisms behind the key back-mixing phenomena of the solids flow.

A cold-flow model, designed, built and operated according to the Glicksman's simplified set of fluid-dynamical scaling laws, is shown to reproduce accurately the fluid dynamics of the >200-MW_{th} CFB boiler used as reference. Experimental campaigns carried out in this cold-scale model, compared to those conducted in an industrial unit, offer a safer environment, wider and more flexible operational ranges, increased measurement possibilities, and lower costs.

The presence of a dense bed results in an increase in solids entrainment from the bottom region with an increase in fluidization velocity, while the absence of a dense bed yields unaltered solids entrainment with increasing fluidization velocity. In the presence of a dense bed, the height of the bed does not show any significant effect on either the solids entrainment or the solids back-mixing rate in the splash zone. The latter is attributed to the attainment (for typical bed heights, i.e., above 0.3 m) of a maximum value for the erupting bubble size, which governs the solids ejection into the splash zone. The solids back-mixing in the transport zone is governed by the transfer of particles through the core-wall layer boundary, which is by DNS modeling shown to be driven by turbophoresis. The solids back-flow at the riser exit increases with increasing gas velocity (thus, with particle velocity) and, therefore, cannot generally be neglected.

A simple Monte Carlo model for the decay coefficient in the splash zone is proposed based on the assumption of gravity-driven ballistic trajectories for the particle clusters and showing good agreement with the measurements. Furthermore, experimental data covering wide ranges of unit size, temperature, and particle size and density have been used to derive an empirical expression to predict the solids entrainment from the bottom region based on dimensionless parameters. Finally, an expression for the decay coefficient in the transport zone is proposed based on a *Sh*-number expression for turbulent internal flow and a turbulence-based model from the literature for the lateral dispersion. After fitting of one coefficient, this expression is able to describe a wide range of experimental data on large-scale CFB boilers taken from the literature.

In addition, it is shown than the knowledge gained and expressions proposed can be combined to generate reliable predictions of the solids flow in CFB furnaces and thus the closure of the mass balance for the solids phase, without the need for any empirical input regarding the flow established inside the furnace. Such predictions are shown to yield good agreement with measurements performed in large-scale CFB boilers, except for those cases in which a dense bed is not present in the bottom region (for which the solids entrainment from the bottom region is significantly lower). With this improvement in the accuracy and validity range of the modeling tools based on the available literature of large-scale CFB furnaces and covering a wide range of operational conditions through experiments in cold flow models, this thesis supports the design and scale-up of CFB processes.

CHAPTER 7
Future work

The following research questions arise from the present work and warrant further investigation. This would provide additional valuable insights into the mechanisms governing the solids flow pattern in large-scale CFB boilers.

- *Solids back-mixing in the splash zone*: How can the solids ejection from the bottom region of the furnace in the absence of a dense bed be described mechanistically?

- *Solids entrainment from the bottom region*: What governs this solids entrainment in the absence of a dense bottom bed and how can it be described? How is this solids entrainment affected by lateral injections of gas for different riser sizes and injection velocities/momentums?

- *Back-flow effect*: Can this local solids back-mixing be generally described through dimensionless numbers (Stokes, Reynolds, Froude) for different conditions, solids properties, and riser sizes and exit geometries?

While this work has focused on the macroscopic features of the solids flow conditions, the possibilities to study the solids flow at smaller scales should be exploited to reveal the underlying phenomena of the solids flow. The fluid dynamically down-scaled unit used in this thesis represents a great opportunity to apply advanced diagnostic techniques in a convenient environment that reproduces the flow conditions in hot large-scale boilers, e.g., the use of magnetic particle tracking to study the fuel mixing [76], and the use of novel radar tomographic tools for resolved measurements of the solids and gas flows. Moreover, CFD modeling is gradually becoming a more useful tool for studying FB units as computational capacity increases, and valuable particle-scale insights can be gained through the use of such modeling to complement the experimental observations.

Nomenclature

a	Decay coefficient of the splash zone	[1/m]
A	Cross-sectional area	[m^2]
C_s	Concentration of particles	[kg/m^3]
$C_{s,entr}$	Entrained concentration at the dense bed	[kg/m^3]
D	Equivalent riser diameter	[m]
d_p	Particle diameter	[μm]
$D_{s,lat}$	Solids macroscopic dispersion in the lateral direction	[m^2/s]
F	Flow of solids	[kg/s]
g	Gravity constant, 9.81	[m/s^2]
G_s	External circulation of solids	[kg/m^{2}s]
$G_{s.entr}^{*}$	Dimensionless entrained flux	[-]
h	Height over distributor plate	[m]
H_b	Dense bed height	[m]
H	Top height of the furnace	[m]
k	Mass transfer coefficient	[m/s]
K	Decay coefficient of the transport zone	[1/m]
k_b	Back-flow ratio	[-]
L^*	Scale factor for length	[-]
W, D	Dimensions of the risers	[m]
l	Length	[m]
m^*	Scale factor for mass	[-]
ΔP	Differential pressure	[Pa]
Pe	Péclet number	[-]
PSD	Particle size distribution	[-]
r	Clustering at a net volumetric rate	[1/s]
Re	Reynolds number	[-]
St	Stokes number	[-]
Sh	Sherwood number	[-]
t	Time	[s]
t^*	Scale factor for time	[-]
u	Fluidization velocity	[m/s]
u_0	Fluidization velocity	[m/s]
u_{mf}	Minimum fluidization velocity	[m/s]
u_t	Terminal velocity	[m/s]
z	Height in the riser	[m]

Greek letters:

$\varnothing_h$	Hydraulic diameter, 4WD/(2W+2D)	[m]
ε_g	Gas fraction	[-]
ρ_g	Density of gas	[kg/m^3]
ρ_s	Density of solid particles	[kg/m^3]
δ_b	Bubble fraction	[-]
ε_s	Particle fraction	[-]
μ_g	Gas viscosity	[Pas]
ξ	Relative gas velocity $\xi = u_g/u_t$	[-]
Φ	Particle sphericity	[-]
ψ	Stokes correction factor	[-]

Subscripts

backflow	Backflow
Bot	Value at the bottom of the furnace
cluster	Bubble eruption into the splash zone
core	Values from the core
DC	Downcomer
disperse	Dispersed phase into the transport zone
entr	Entrained solids from bottom
Exit	Value at the cyclone exit
g	Gas
Hb	Values in the dense bed
lat	Lateral dispersion
layer	Wall layer
Max	Maximum value
Min	Minimum value
p	Particle
Ref	Reference values measured in the range of h=0.1–1.6 m
Riser	Riser, values measured for the whole furnace
s	Solids
Top	Value at the top of the furnace

References

1. IEA, *Energy, Climate Change and Environment 2016 Insights*, I.E. Agency, Editor. 2016: Paris, France.
2. Leckner, B., L. Thorson, J. Kjärstad, and F. Johnsson, *Utilization of fluidized bed boilers ---a worldwide overview*, in *Developments in Fluidized Bed Conversion 2011 to 2016*. 2016, IEA-FBC TCP: Presented at IEA-FBC 73rd Technical Meeting, Tokyo, Japan (December 2016).
3. Koornneef, J., M. Junginger, and A. Faaij, *Development of fluidized bed combustion—An overview of trends, performance and cost.* Progress in Energy and Combustion Science, 2007. **33**(1): p. 19-55.
4. Obernberger, I., *Decentralized biomass combustion: state of the art and future development.* Biomass Bioenergy, 1998. **14**(1): p. 33-56.
5. Leckner, B., *Fluidized bed combustion: mixing and pollutant limitation.* Progress in Energy and Combustion Science, 1998. **24**(1): p. 31-61.
6. Adanez, J., A. Abad, F. Garcia-Labiano, P. Gayan, and F. Luis, *Progress in chemical-looping combustion and reforming technologies.* Progress in energy and combustion science, 2012. **38**(2): p. 215-282.
7. Thunman, H., M. Seemann, T. Berdugo Vilches, J. Maric, D. Pallares, H. Ström, G. Berndes, P. Knutsson, A. Larsson, and C. Breitholtz, *Advanced biofuel production via gasification–lessons learned from 200 man-years of research activity with Chalmers' research gasifier and the GoBiGas demonstration plant.* Energy Science Engineering, 2018. **6**(1): p. 6-34.
8. Gómez-Barea, A. and B. Leckner, *Modeling of biomass gasification in fluidized bed.* Progress in Energy Combustion Science, 2010. **36**(4): p. 444-509.
9. Perejón, A., L.M. Romeo, Y. Lara, P. Lisbona, A. Martínez, and J.M. Valverde, *The Calcium-Looping technology for CO2 capture: On the important roles of energy integration and sorbent behavior.* Applied Energy, 2016. **162**: p. 787-807.
10. Rydén, M., M. Hanning, A. Corcoran, and F. Lind, *Oxygen carrier aided combustion (OCAC) of wood chips in a semi-commercial circulating fluidized bed boiler using manganese ore as bed material.* Applied Sciences, 2016. **6**(11): p. 347.
11. Pardo, P., A. Deydier, Z. Anxionnaz-Minvielle, S. Rougé, M. Cabassud, and P. Cognet, *A review on high temperature thermochemical heat energy storage.* Renewable Sustainable Energy Reviews, 2014. **32**: p. 591-610.
12. Flegkas, S., F. Birkelbach, F. Winter, H. Groenewold, and A. Werner, *Profitability Analysis and Capital Cost Estimation of a Thermochemical Energy Storage System Utilizing Fluidized Bed Reactors and the Reaction System MgO/Mg (OH) 2.* Energies, 2019. **12**(24): p. 4788.
13. Espatolero, S. and L.M. Romeo, *Optimization of oxygen-based CFBC technology with CO2 capture.* Energy Procedia, 2017. **114**: p. 581-588.
14. Mathekga, H., B. Oboirien, and B.C. North, *A review of oxy-fuel combustion in fluidized bed reactors.* International Journal of Energy Research, 2016. **40**(7): p. 878-902.
15. Leckner, B., P. Szentannai, and F. Winter, *Scale-up of fluidized-bed combustion–A review.* Fuel, 2011. **90**(10): p. 2951-2964.
16. Myöhänen, K. and T. Hyppänen, *A three-dimensional model frame for modelling combustion and gasification in circulating fluidized bed furnaces.* International Journal of Chemical Reactor Engineering, 2011. **9**(1).
17. Johnsson, F. and B. Leckner. *Vertical distribution of solids in a CFB-furnace.* in *CONF-950522.* 1995. American Society of Mechanical Engineers, New York, NY (United States).
18. Werdermann, C.C., *Feststoffbewegung und Wärmeübergang in zirkulierenden Wirbelschichten von Kohlekraftwerken.* 1993: Shaker.
19. Couturier, M., B. Doucette, D. Stevens, S. Poolpol, and V. Razbin. *Temperature, gas concentration and solid mass flux profiles within a large circulating fluidized bed combustor.* in *11th International Conference on FBC, ASME.* 1991. Montreal.
20. Johnsson, F., W. Zhang, and B. Leckner. *Characteristics of the formation of particle wall-layers in CFB boilers.* in *Proceedings of the second international conference on multiphase flow.* 1995. The Japan Society of Multiphase Flow Nagoya.
21. Lafanechere, L. and L. Jestin, *Study of a circulating fluidized bed furnace behavior in order to scale it up to 600 MWe.* 1995, American Society of Mechanical Engineers, New York, NY (United States).
22. Leretaille, P., J. Werther, P. Briand, and D. Montat, *Modeling of hydrodynamics of large scale atmospheric circulating fluidized bed coal combustors.* 1999, Technical Univ. Hamburg-Harburg, Hamburg (DE).
23. Johansson, A., *Solids flow pattern in circulating fluidized-bed boilers.* 2005.

24.   Mirek, P., *Influence of the model scale on hydrodynamic scaling in CFB Boilers.* Brazilian Journal of Chemical Engineering, 2016. **33**(4): p. 885-896.

25.   Yang, H., G. Yue, X. Xiao, J. Lu, and Q. Liu, *1D modeling on the material balance in CFB boiler.* Chemical Engineering Science, 2005. **60**(20): p. 5603-5611.

26.   Pallarès, D., *Fluidized Bed Combustion: Modeling and Mixing.* 2008, Chalmers University of Technology.

27.   Myöhänen, K., *Modelling of combustion and sorbent reactions in three-dimensional flow environment of a circulating fluidized bed furnace.* Acta Universitatis Lappeenrantaensis, 2011.

28.   Hannes, J.P., *Mathematical modelling of circulating fluidized bed combustion.* 1998.

29.   Wischnewski, R., L. Ratschow, E.-U. Hartge, and J. Werther, *Reactive gas–solids flows in large volumes—3D modeling of industrial circulating fluidized bed combustors.* Particuology, 2010. **8**(1): p. 67-77.

30.   Wen, C. and L. Chen, *Fluidized bed freeboard phenomena: entrainment and elutriation.* AIChE Journal, 1982. **28**(1): p. 117-128.

31.   Kunii, D. and O. Levenspiel, *Entrainment of solids from fluidized beds I. Hold-up of solids in the freeboard II. Operation of fast fluidized beds.* Powder Technology, 1990. **61**(2): p. 193-206.

32.   Johnsson, F., B. Leckner, and A. Vrager. *Solids flow pattern in the exit region of a CFB--Furnace influence of exit geometry.* in *15th Int. Conf. on Fluidized Bed Combustion.* 1999. Savannah (Georgia, USA). Chalmers Univ. of Technology, Göteborg (SE).

33.   Davidson, J., *Circulating fluidised bed hydrodynamics.* Powder Technology, 2000. **113**(3): p. 249-260.

34.   Johnsson, F., A. Svensson, S. Andersson, and B. Leckner, *Fluidization Regimes in Boilers,* in *Fluidization VIII.* 1995, International Symposium of the Engineering Foundation: Tours, France. p. 129-136.

35.   Sasic, S., B. Leckner, and F. Johnsson, *Fluctuations and waves in fluidized bed systems: the influence of the air-supply system.* Powder technology, 2005. **153**(3): p. 176-195.

36.   Svensson, A., F. Johnsson, and B. Leckner, *Bottom bed regimes in a circulating fluidized bed boiler.* International Journal of Multiphase Flow, 1996. **22**(6): p. 1187-1204.

37.   Svensson, A., F. Johnsson, and B. Leckner, *Fluidization regimes in non-slugging fluidized beds: the influence of pressure drop across the air distributor.* Powder Technology, 1996. **86**(3): p. 299-312.

38.   Pallares, D. and F. Johnsson, *Macroscopic modelling of fluid dynamics in large-scale circulating fluidized beds.* Progress in Energy and Combustion Science, 2006. **32**(5-6): p. 539-569.

39.   Kunii, D. and O. Levenspiel, *Fluidization engineering.* 1991.

40.   Johansson, A., F. Johnsson, and B. Leckner, *Solids back-mixing in CFB boilers.* Chemical Engineering Science, 2007. **62**(1-2): p. 561-573.

41.   Gayan, P., J. Adanez, F. Luis, F. García-Labiano, A. Cabanillas, A. Bahillo, M. Aho, and K. Veijonen, *Circulating fluidised bed co-combustion of coal and biomass.* Fuel, 2004. **83**(3): p. 277-286.

42.   Löffler, G., S. Kaiser, K. Bosch, and H. Hofbauer, *Hydrodynamics of a dual fluidized-bed gasifier—Part I: simulation of a riser with gas injection and diffuser.* Chemical Engineering Science, 2003. **58**(18): p. 4197-4213.

43.   Adanez, J., P. Gayan, L. De Diego, F. Garcia-Labiano, and A. Abad, *Combustion of wood chips in a CFBC. Modeling and validation.* Industrial engineering chemistry research, 2003. **42**(5): p. 987-999.

44.   Karlsson, T., X. Liu, D. Pallarès, and F. Johnsson, *Solids circulation in circulating fluidized beds with low riser aspect ratio and varying total solids inventory.* Powder Technology, 2017. **316**: p. 670-676.

45.   Djerf, T., D. Pallarès, and F. Johnsson, *Bottom-bed fluid dynamics–Influence on solids entrainment.* Fuel Processing Technology, 2018. **173**: p. 112-118.

46.   Lyngfelt, A. and B. Leckner, *A 1000 MWth boiler for chemical-looping combustion of solid fuels– Discussion of design and costs.* Applied Energy, 2015. **157**: p. 475-487.

47.   Gómez-Barea, A. and B. Leckner, *Estimation of gas composition and char conversion in a fluidized bed biomass gasifier.* Fuel, 2013. **107**: p. 419-431.

48.   Zhang, W., F. Johnsson, and B. Leckner, *Fluid-dynamic boundary layers in CFB boilers.* Chemical Engineering Science, 1995. **50**(2): p. 201-210.

49.   Edvardsson, E., L.-E. Åmand, H. Thunman, B. Leckner, and F. Johnsson. *Measuring the external solids flux in a CFB boiler.* in *Proceedings of the 19th FBC Conferance.* 2006. Vienna Austria.

50.   Werther, J. *Fluid mechanics of large-scale CFB units.* in *Proceedings of 4th International CFB Conference.* 1993.

51.   Van der Meer, E., R. Thorpe, and J. Davidson, *Flow patterns in the square cross-section riser of a circulating fluidised bed and the effect of riser exit design.* Chemical Engineering Science, 2000. **55**(19): p. 4079-4099.

52.   Senior, R.C. and C. Brereton, *Modelling of circulating fluidised-bed solids flow and distribution.* Chemical Engineering Science, 1992. **47**(2): p. 281-296.

53. Yue, G., J. Lu, H. Zhang, H. Yang, J. Zhang, Q. Liu, Z. Li, E. Joos, and P. Jaud. *Design theory of circulating fluidized bed boilers*. in *18th International Conference on Fluidized Bed Combustion*. 2005. American Society of Mechanical Engineers.

54. Redemann, K., E.-U. Hartge, and J. Werther, *A particle population balancing model for a circulating fluidized bed combustion system.* Powder technology, 2009. **191**(1-2): p. 78-90.

55. Glicksman, L.R., *Scaling relationships for fluidized beds.* Chemical Engineering Science, 1984. **39**(9): p. 1373-1379.

56. Markström, P. and A. Lyngfelt, *Designing and operating a cold-flow model of a 100 kW chemical-looping combustor.* Powder Technology, 2012. **222**: p. 182-192.

57. Glicksman, L., M. Hyre, and P. Farrell, *Dynamic similarity in fluidization.* International Journal of Multiphase Flow, 1994. **20**: p. 331-386.

58. Horio, M., H. Ishii, Y. Kobukai, and N. Yamanishi, *A scaling law for circulating fluidized beds.* Journal of Chemical Engineering of Japan, 1989. **22**(6): p. 587-592.

59. Glicksman, L., M. Hyre, and K. Woloshun, *Simplified scaling relationships for fluidized beds.* Powder Technology, 1993. **77**(2): p. 177-199.

60. Van der Meer, E., R. Thorpe, and J. Davidson, *Dimensionless groups for practicable similarity of circulating fluidised beds.* Chemical Engineering Science, 1999. **54**(22): p. 5369-5376.

61. Sette, E., D. Pallarès, and F. Johnsson, *Experimental quantification of lateral mixing of fuels in fluid-dynamically down-scaled bubbling fluidized beds.* Applied Energy, 2014. **136**: p. 671-681.

62. Schöny, G., E. Zehetner, J. Fuchs, T. Pröll, G. Sprachmann, and H. Hofbauer, *Design of a bench scale unit for continuous CO2 capture via temperature swing adsorption—Fluid-dynamic feasibility study.* Chemical Engineering Research Design, 2016. **106**: p. 155-167.

63. Sasic, S., F. Johnsson, and B. Leckner, *Interaction between a fluidized bed and its air-supply system: Some observations.* Industrial & Engineering Chemistry Research, 2004. **43**(18): p. 5730-5737.

64. Zhang, W. and F. Johnsson, *Fluid-dynamic boundary layers in circulating fluidized bed boilers*, A91-193, Editor. 1991: Dept. of Energy Convrsion, Chalmers University of Technology, Göteborg.

65. Djerf, T., D. Pallarés, and F. Johnsson, *Solids flow patterns in large-scale Circulating Fluidised Bed boilers: experimental evaluation under fluid-dynamically down-scaled conditions* Chemical Engineering Science, 2020.

66. Fung, A.S. and F. Hamdullahpur, *A gas and particle flow model in the freeboard of a fluidized bed based on bubble coalescence.* Powder Technology, 1993. **74**(2): p. 121-133.

67. Santana, D., S. Nauri, A. Acosta, N. García, and A. Macías-Machín, *Initial particle velocity spatial distribution from 2-D erupting bubbles in fluidized beds.* J Powder Technology, 2005. **150**(1): p. 1-8.

68. Rajiv, K. and M.K. Lal, *Turbophoresis*, in *Developments in Surface Contamination and Cleaning - Particle Deposition, Control and Removal*. 2010: William Andrew Publishing.

69. Caporaloni, M., F. Tampieri, F. Trombetti, and O. Vittori, *Transfer of particles in nonisotropic air turbulence.* Journal of the atmospheric sciences, 1975. **32**(3): p. 565-568.

70. Mortimer, L., D. Njobuenwu, and M. Fairweather, *Near-wall dynamics of inertial particles in dilute turbulent channel flows.* Physics of Fluids, 2019. **31**(6): p. 063302.

71. Johnsson, F., R. Zijerveld, J.v. Schouten, C. Van den Bleek, and B. Leckner, *Characterization of fluidization regimes by time-series analysis of pressure fluctuations.* International journal of multiphase flow, 2000. **26**(4): p. 663-715.

72. Lücke, K., *On the Influence if Mixing in the Performance of Large-Scale Atmospheric Circulating Fluidized Bed Combustors*. 2003, Technischen Universit at Hamburg: Shaker.

73. Palchonok, G., F. Johnsson, and B. Leckner, *Estimates of turbulence effects in CFB boilers.* Circulating Fluidized Bed Technology V, Science Press, Beijing, 1996: p. 440-445.

74. Israel, R. and D.E. Rosner, *Use of a generalized Stokes number to determine the aerodynamic capture efficiency of non-Stokesian particles from a compressible gas flow.* Aerosol Science Technology, 1982. **2**(1): p. 45-51.

75. Serafini, J.S., *Impingement of water droplets on wedges and double-wedge airfoils at supersonic speeds*. 1954: NASA Technical Report Server.

76. Köhler, A., D. Pallarés, and F. Johnsson, *Magnetic tracking of a fuel particle in a fluid-dynamically down-scaled fluidised bed.* Fuel Processing Technology, 2017. **162**: p. 147-156.